Review

Optical Applications of CuInSe₂ Colloidal Quantum Dots

Published as part of ACS Omega virtual special issue "At the Speed of Light: Recent Advances in Optoelectronics".

Song Chen, Bingqian Zu, and Liang Wu*

Read Online

ACCESS | Metrics & More | Article Recommendations

ABSTRACT: The distinctive chemical, physical, electrical, and optical properties of semiconductor quantum dots (QDs) make them a highly fascinating nanomaterial that has been extensively studied. The CuInSe₂ (CIS) QDs demonstrates great potential as a nontoxic alternative to CdSe and PbSe QDs for realizing high-performance solution-processed semiconductor devices. The CIS QDs show strong light absorption and bright emission across the visible and infrared spectrum and have been designed to exhibit optical gain. The special characteristics of these properties are of great significance in the fields of solar energy conversion, display, and electronic devices. Here, we present a comprehensive overview of the potential applications of colloidal CIS QDs in various fields, with a particular focus on solar energy conversion (such as QD solar cells, QD-sensitized solar cells, and QD luminescence solar concentrators), solar-to-hydrogen production (such as photocatalytic and photoelectrochemical H₂ production), and QD electronics (such as QD transistors, QD light-emitting diodes, and QD photodetectors). Furthermore, we offer our insights into the current challenges and future opportunities associated with CIS QDs for further research.
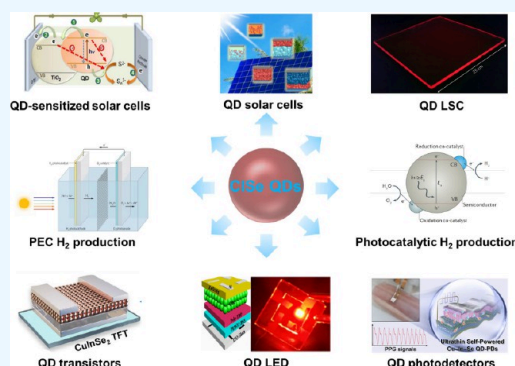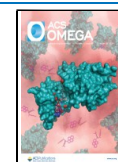
1. INTRODUCTION

The electronic and optical properties of bulk semiconductors are usually regulated via crystal structure, composition, and impurities. Nevertheless, the electron energy level transitions from quasi-continuous to discrete and confinement arises when the size of the semiconductor reaches a specific value known as the exciton Bohr radius. The quantum-confined semiconductors commonly exhibit size-dependent electronic and optical properties, which bring about extra degrees of tunability compared with bulk semiconductors. The quantum-confined materials can be classified into zero-dimensional (0D), one-dimensional (1D), and two-dimensional (2D), including quantum dots (QDs), quantum wires/rods, and quantum wells, respectively.[1−3]

The QD is a semiconductor nanostructure that binds excitons in three spatial directions. The QD is a significant low-dimensional semiconductor material, characterized by its dimensions in all three directions being no more than twice the excitonic Bohr radius of the corresponding semiconductor. Typically, QDs exhibit a spherical or quasi-spherical shape, with diameters ranging from 2 to 20 nm. In QDs, holes and electrons exhibit a discrete (quantized) and analogous density of states (DOS).[4−6] The bandgap of QDs increases due to the quantum confinement, leading to a blue shift in both absorption and emission spectra.[7] The excited electron exhibits a strong interaction with the remaining hole. The spin-exchange coupling

and Coulomb attraction synergistically generate highly localized excitons (electron−hole pairs). The close proximity of charge carriers in QDs leads to heightened many-body phenomena that impact their optical and electronic properties.[8]

Importantly, colloidal quantum dots (CQDs) that are usually synthesized via wet-chemical approaches are solution-processed nanocrystals with diameters below 20 nm. Since the first report in the 1980s,[9] numbers of semiconductor CQDs have been developed, such as groups II−VI,[10] III−V,[11] I−III−VI₂,[12] and I−II−III-VI.[13] The CuInSe₂ (CIS) CQDs among the I−III−VI QDs have garnered increasing attention due to its substantial exciton Bohr radius of ca. 10.6 nm, which facilitates the regulation of the energy bandgaps across a broad spectrum of light absorption ranging from ultraviolet to near-infrared regions.[14−16] Furthermore, the band structure related to composition and its special defect tolerance facilitate convenient tailoring of band alignment according to the practical applications.[17−19] The use of CIS QDs as a nontoxic alternative

to CdSe and PbSe QDs has gained widespread popularity in the field of high-performance solution-processed semiconductor devices.[17,20−22]

The use of CIS CQDs offers opportunities for the production of high-efficiency and flexible devices through large-area, low-temperature, solution-based approaches that replace costly high-temperature, high-vacuum device fabrication processes.[23−25] In this review, we examine the utilization of CIS CQDs in the development of solar energy conversion, displays, and electronic devices. We focus on their applications in QD solar cells, QD-sensitized solar cells (QDSSCs), QD luminescence solar concentrators (LSCs), photocatalytic and photoelectrochemical (PEC) H$_2$ production, QD transistors, QD light-emitting diodes (LEDs), and QD photodetectors (Figure 1). Furthermore, we explore the emerging opportunities for CIS CQDs and discuss the challenges toward practical applications.
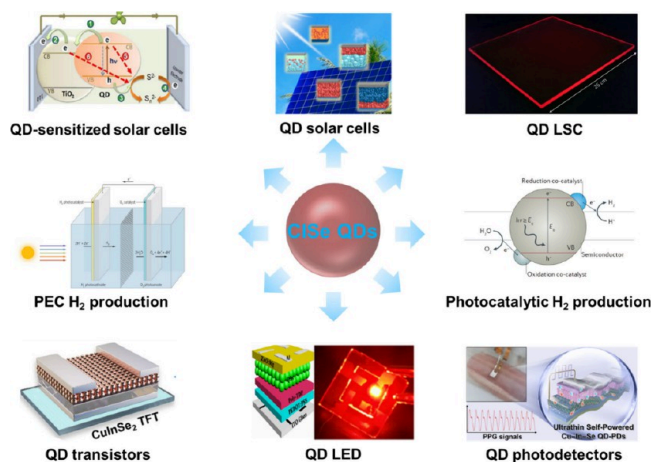

Figure 1. Graphical illustration of some optical applications of CIS QDs.[26−33] Some of the subgraphics are reprinted in part with permission from the following: ref 26, copyright 2015 American Chemical Society; ref 27, copyright 2013 Taylor & Francis; ref 28, copyright 2023 American Chemical Society; ref 29, copyright 2018 The Optical Society; ref 30, copyright 2021 American Chemical Society; ref 31, copyright 2016 American Association for the Advancement of Science; ref 32, copyright 2017 Springer Nature; ref 33, copyright 2017 Springer Nature.

2. OPTICAL APPLICATIONS OF CIS CQDS

2.1. QD Solar Cells. QD solar cells have attracted extensive interests as low-cost solution-processable alternative photo-voltaic devices before the creation and rise of perovskite solar cells.[34−36] Compared with traditional thin-film-based perovskite solar cells, QD solar cells possess unique advantages. They are processable and compatible with greener solvents (e.g., octane, hexane, toluene, etc.).[37−39] Moreover, the compatibility of QDs with greener solvents is more important for large-scale industrial fabrication compared to perovskites.[40] Additionally, the low-cost solution process is one of the most attractive particularities of QD solar cells as a substitute to silicon photovoltaics.[12,41] With constant development, QD solar cells have reached 18.1% efficiency in 2020.[34]

The lead chalcogenide family (PbS and PbSe) had dominated the QD photovoltaic technology until the emergence of I−III−VI CQDs.[24,42,43] The CIS CQDs incorporate several key features of binary metal chalcogenide QDs, including surface passivation by ligands and quantum confinement, while also

possessing exceptional absorption properties similar to bulk CIS.[16] CIS is a crucial material for photovoltaic devices, exhibiting the highest efficiency of over 20% specifically in thin film solar cells.[44,45] However, the power conversion efficiency (PCE) of photovoltaic devices fabricated from ink-deposited CIS CQDs is just over 3%, astricted by poor charge transport.[42,46,47] Typically, ink-deposited CQDs are sintered into polycrystalline films by annealing under selenium vapor at high temperature (>500 °C) to achieve much higher efficiencies.[48,49] Korgel and coauthors reported a nanocrystal film processing technique—photonic curing—to replace high-temperature selenization to improve charge transport in the QD films (Figure 2a).[43] The photovoltaic devices were fabricated by
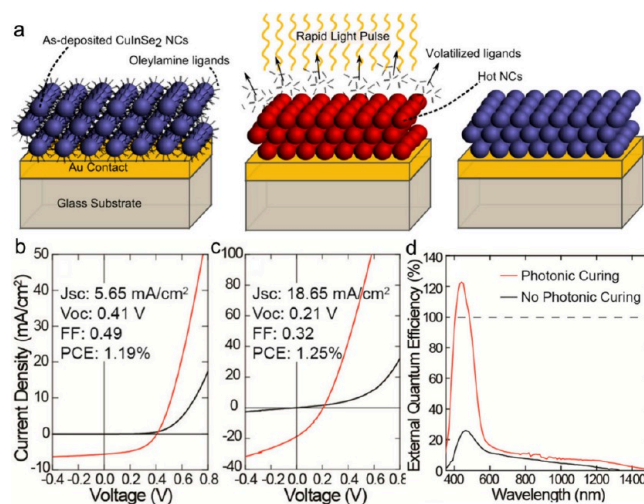

Figure 2. (a) Schematic illustration the removing OLA from the CIS nanocrystal film via photonic curing. (b,c) Current−voltage curves of devices made with the CIS CQDs before and after photonic curing with 2.2 J/cm^2 pulse fluence. (d) EQE measurements for CIS QD devices under white light bias (50 mW/cm^2) before (black curve) and after (red curve) photonic curing with 2.2 J/cm^2 pulse fluence.[43] Reproduced with permission from ref 43. Copyright 2013 American Chemical Society.

spray deposition of CIS CQD toluene dispersions on Au-coated glass substrates. Then, the QD films were cured with a PluseForge 3300 tool in a closed chamber with a quartz window using pulsed light from a xenon flash lamp.

Although the CIS QD films are cured with a 2.2 J/cm^2 pulse fluence, the photovoltaic devices fabricated with these cured QDs exhibited unsatisfactory performance. As shown in Figure 2b,c, the PCE of the photovoltaic devices fabricated with cured QDs is 1.25%, which is similar to that of the devices fabricated with CQDs without photocuring (1.19%). However, the devices exhibit a noticeable decrease in the open-circuit voltage and a significant enhancement in the short-circuit current after undergoing photonic curing. External quantum efficiency (EQE) characterizations revealed that the predominant increase in short-circuit current occurred within the short wavelength range (<600 nm). Due to the extraction of multiexcitons, the peak EQE of the devices fabricated with cured QDs reached 123%, which is much higher than that of the CIS QD solar cells without photonic curing.

2.2. QD Luminescent Solar Concentrators. The utilization of solar power generation presents an efficient solution to addressing the energy crisis. The primary strategies for cost reduction in solar electricity involve enhancing the
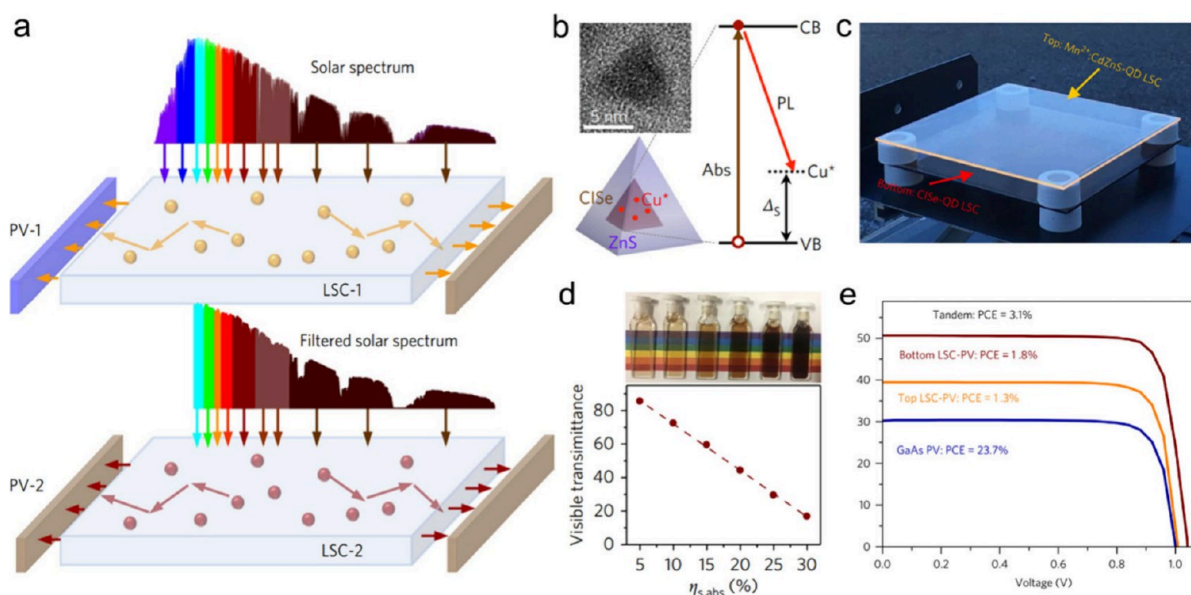
Figure 3. (a) Schematic illustration of the solar-spectrum splitting in a tandem LSC. (b) HRTEM image of an individual CIS/ZnS QD and schematic illustration of electronic states and optical transitions according to light absorption (brown arrow) and PL emission (red arrow). (c) Photograph of a tandem LSC (ca. 232 cm^{2-}) with a M^{2+} doped $Cd_xZn_{1-x}S$ QD top layer and a CISe QD bottom layer. (d) Solution samples of CIS/ZnS QDs with different concentrations and the corresponding visible transmittances. (e) Current density vs. voltage ($J-V$) characteristics.[53] Reproduced with permission from ref 53. Copyright 2018 Springer Nature.

efficiencies of solar cells and optimizing manufacturing and installation processes to minimize expenses. Utilizing cheap, large-area solar radiation collectors based on the LSCs technology presents a promising opportunity to lower the price of solar energy.[50−52] LSCs are constructed with a slab of an transparent material containing highly emissive fluorophores, such as CQDs (Figure 3a).[53] These LSCs can be integrated with Si-solar cells in edge as well as used as semitransparent "solar windows".[54,55] The fluorophores absorb the solar photons and subsequently emit at longer wavelengths, which are then waveguided to the Si-solar cells located at the edges to generate electricity. Moreover, the LSC technology can be utilized for the fabrication of novel devices, such as lightweight optical antennas designed for space applications and spectral reshapers intended for photobiology and photochemistry applications.[56,57]

Since the initial proposal of LSCs as cost-effective alternatives to silicon solar cells in 1976,[58] an increasing number of researchers have been focusing their attention on LSCs and specifically studying dye molecules.[59,60] However, the general dyes have limited solar spectral coverage and exhibit low PL efficiencies at the near-infrared wavelengths—which are most suitable for coupling to silicon photovoltaics—as well as significant reabsorption losses. Due to the unrivaled tunability of emission spectra in the visible and NIR regions associated with high PL quantum yields and high photostability, CQDs represent a fascinating emerging category of LSC emitters.[61−63] In addition, the CQDs with tunable bandgaps are also well suited for fabrication of multilayered LSCs, where each layer is specifically constructed to absorb the different parts of the solar spectrum (Figure 3a).

Klimov and coauthors fabricated a large-area and high-efficiency tandem LSC, where one layer absorbs the visible light and another absorbs the NIR.[53] CIS cores with a size of 3.1 ± 0.5 nm were synthesized and subsequently coated with a thick ZnS layer to fabricate the top LSC layer. This was done due to the strong absorbance in the solar spectrum and high PL quantum

yield (65−75%) (Figure 3b). The obtained large-area CIS/ZnS LSC (15.24×15.24 cm^2) appears dark to an observer, which has a total sunlight absorptance of 28% (Figure 3c) and a corresponding visible transmittance of 23% (Figure 3d). Then, the M^{2+} doped $Cd_xZn_{1-x}S$ CQDs with absorption in the ultraviolet region and a high PL quantum yield (78%) were utilized to fabricate the top LSC layer (Figure 3b). As shown in Figure 3e, the PCEs of the top and bottom layers are 1.3% and 1.8%, respectively. The tandem QD LSC shows a high optical quantum efficiency of 6.4% under sunlight illumination and PCE of 3.1%.

2.3. QD-Sensitized Solar Cells. As a cost-effective alternative to film photovoltaics, semiconductor QDSSCs have drawn significant attention recently and exhibit great potentials for the next generation of photovoltaics.[64−66] QDSSCs derived from dye-sensitized solar cells were first reported by O'Regan and Gratzel in 1991.[67] CQDs have been utilized to replace organic dyes as the photosensitizer due to their electrical and optical properties, such as size-dependent bandgaps, higher stability toward water and oxygen, larger extinction coefficient, and multiple exciton generation with single-photon absorption.[27,68] Due to the multiple exciton generation, the theoretical PCE of QDSSCs reaches up to 42%, which surpasses the efficiency of 31% for semiconductor solar cells.[69]

For large-scale applications, the integration of QDSSC technologies has the benefits of useful device construction and solution-processable production owing to their considerably simple device manufacturing approaches and suitable structure.[71,72] Since the report of the first certified QDSSCs in 2013, the PCE of QDSSCs has increased dramatically to >13% in recent years.[73−75] Similar to the initial certified QDSSCs, the champion QDSSCs utilize the less-toxic I−III−VI$_2$ CQDs with a high absorption coefficient and near optimal band gap energy (1.0−1.5 eV).[76−78] Chang and coauthors used aqueous synthesized Mn-doped CIS CQDs as the photosensitizer in QDSSCs (Figure 4a), exhibiting Mn concentration dependent
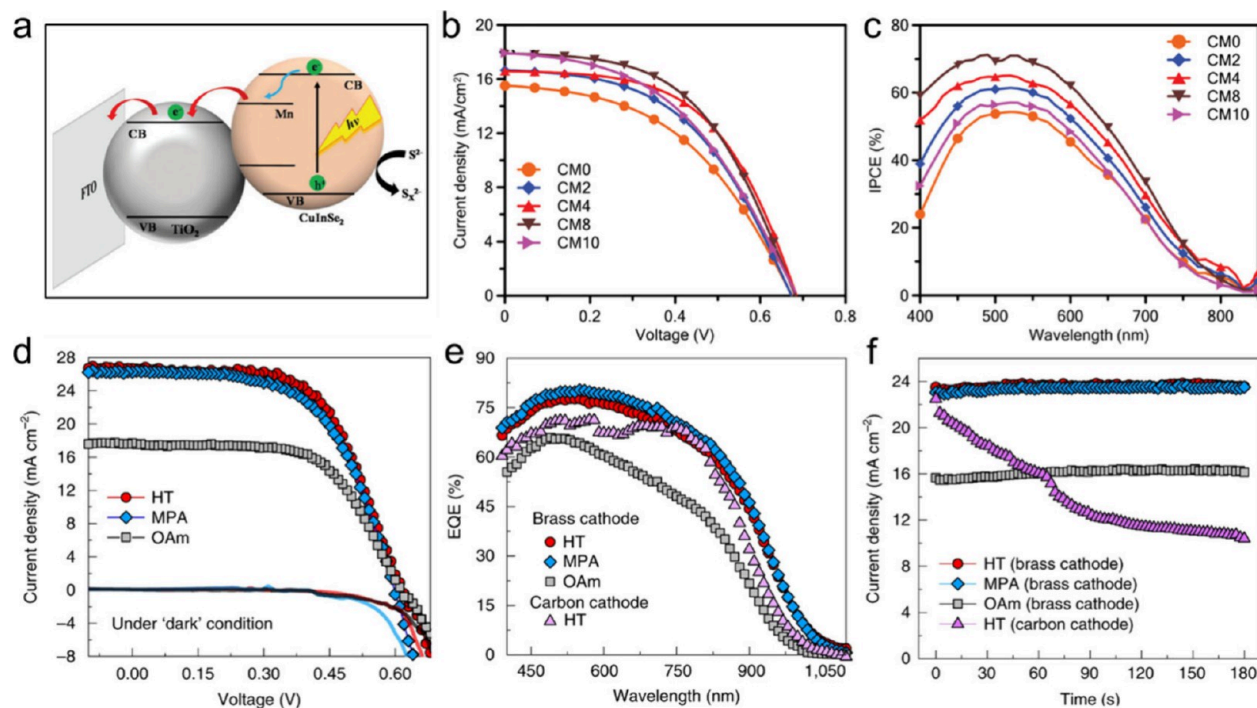
Figure 4. (a) Schematic showing the mechanism of electron injection in Mn-doped CIS QDSSCs. (b,c) $J-V$ characteristics and IPCE spectra of Mn-doped CIS CQDs.[70] Reproduced with permission from ref 70. Copyright 2019 Royal Society of Chemistry. (d,e) $J-V$ characteristics and corresponding EQE of the brass-cathode-based solar cells made of CQDs with HT, MPA, and OAm ligands. (f) Temporal evolution of the current density of the brass- and mesoporous-carbon-based solar cells investigated under AM 1.5 G illumination, with the bias set to V_{max}. V_{max} = 0.56, 0.38, and 0.39 V for the QDs capped with OAm, MPA, and HT, respectively.[19] Reproduced with permission from ref 19. Copyright 2020 Springer Nature.

performances.[70] The short-circuit current increased with the incorporation concentration of Mn into CIS QDs (Figure 4b), which is attributed to the effective injection of excited electrons from CIS QDs into TiO_2 and the resulting higher lifetime of electrons, probably via the formed Mn midgap in the CIS band structure (Figure 4a). The Mn-doped CIS QDSSCs show a maximum PCE of 6.28% (Figure 4c) due to the combination of higher light-absorption efficiency, slower carrier recombination, and a longer lifetime of electrons.

In addition, surface treatments and linking strategies are beneficial for the formation of strong coupling of QDs to the TiO_2 electrode which can usefully eliminate surface-related intragap defects and accelerate the electron migration rate, thereby achieving excellent PV performance. Du and coauthors studied the carrier dynamics in TiO_2-electrode-coupled Zn-doped CIS QDs with "linking" and "nonlinking" surface ligands and correlated the spectroscopic observations with the photovoltaic performance of the QDs. They regulated the defect-related relaxation rate and QD-to-TiO_2 electrode electron transfer rate through the use of surface ligands with diverse lengths and binding forces. Moreover, these ligands do not introduce any electrostatic or steric limitations, but rather facilitate the formation of a compact layer of QDs on the surface of the photoelectrode. They obtained a high short-circuit current of >26 mA cm^{-2} (Figure 4d), which is similar to that of the best reported QDSSCs.[76] The developed QDSSCs show a high reproducible PCE of 9−10% and a high EQE of ~85% (Figure 4e). The excellent performances are attributed to the peculiar photoconversion mechanism involving two types of intragap states: native Cu^+ hole-trapping defects and surface-located electron traps, which can mediate QD interactions with the electrolyte and the TiO_2 electrode, respectively. Moreover,

the stability of solar cells utilizing a brass electrode is significantly enhanced, in comparison to devices employing a carbon cathode. The performance of the system remains stable without any noticeable degradation during 3 min long stability tests (Figure 4f). The findings suggest that the degradation of the electrolyte in this particular case is effectively suppressed. This is achieved through chemical transformations involving copper species, which mediate the reduction of polysulfides on the cathode side of the device and consequently prevent the formation of sulfur radicals.

2.4. PEC H_2 Production. Hydrogen energy serves as a widely used green secondary energy. However, it is noteworthy that there is almost no existence of hydrogen on Earth. Generally, the production of H_2 is achieved through the decomposition of hydrogen-containing substances, such as water. PEC H_2 production is a simple, cost-effective, sustainable, and environmentally benign method to realize solar-to-hydrogen conversion.[79−82] Semiconductor QDs are deemed to be promising materials for PEC H_2 production due to their unique electronic and optical properties, such as high optical absorption coefficient, tunable band gap and band structure, and potential multiple exciton generation.[77,83] Furthermore, the utilization of QDs to sensitize metal-oxide semiconductors is one of the most promising methods for effective PEC hydrogen generation.[84−88] To date, the QDs mainly investigated for PEC H_2 production contain toxic elements such as Cd or Pb, limiting the applications in practice owing to the associated environmental issues.[85,89]

Heavy-metal-free I−III−VI CQDs are emerging as promising alternative materials and have been extensively utilized for PEC H_2 production due to their low toxicity, wide absorption region, and high light extinction coefficient.[91−95] Many efforts have
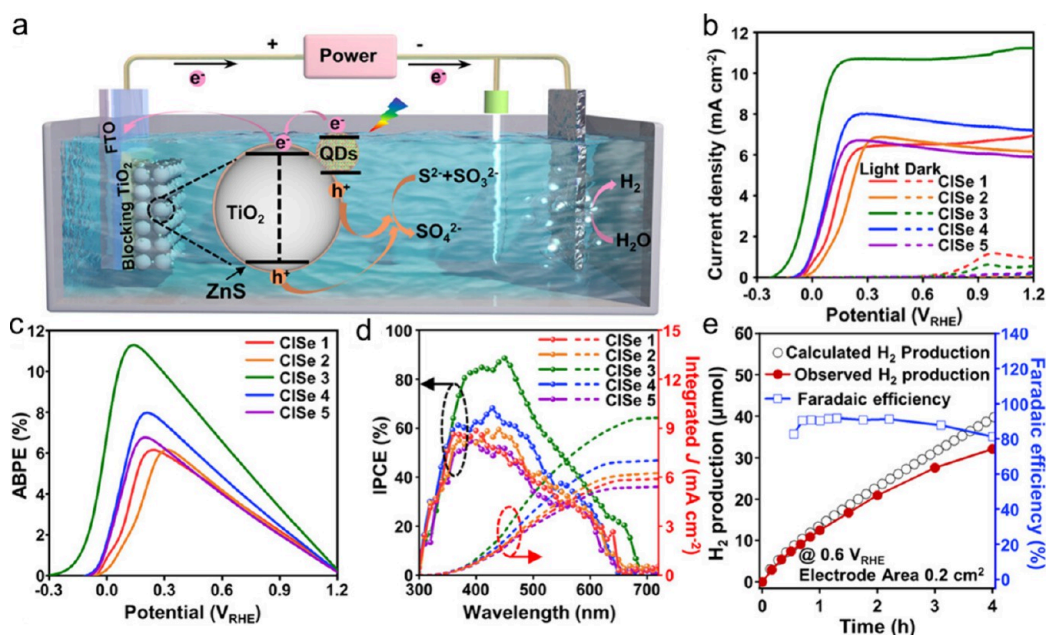
Figure 5. (a) Schematic illustration of the PEC H_2 production using a CIS QDs/TiO_2 photoanode. (b−d) J−V curves, ABPE curves, and IPCE spectra of CIS QDs/TiO_2 photoanodes. (e) H_2 evolution over time measured at 0.6 V vs RHE, calculated Faradaic efficiency, and calculated theoretical H_2 yield of the CIS 3/TiO_2 photoanode.[90] Reproduced with permission from ref 90. Copyright 2023 Wiley.
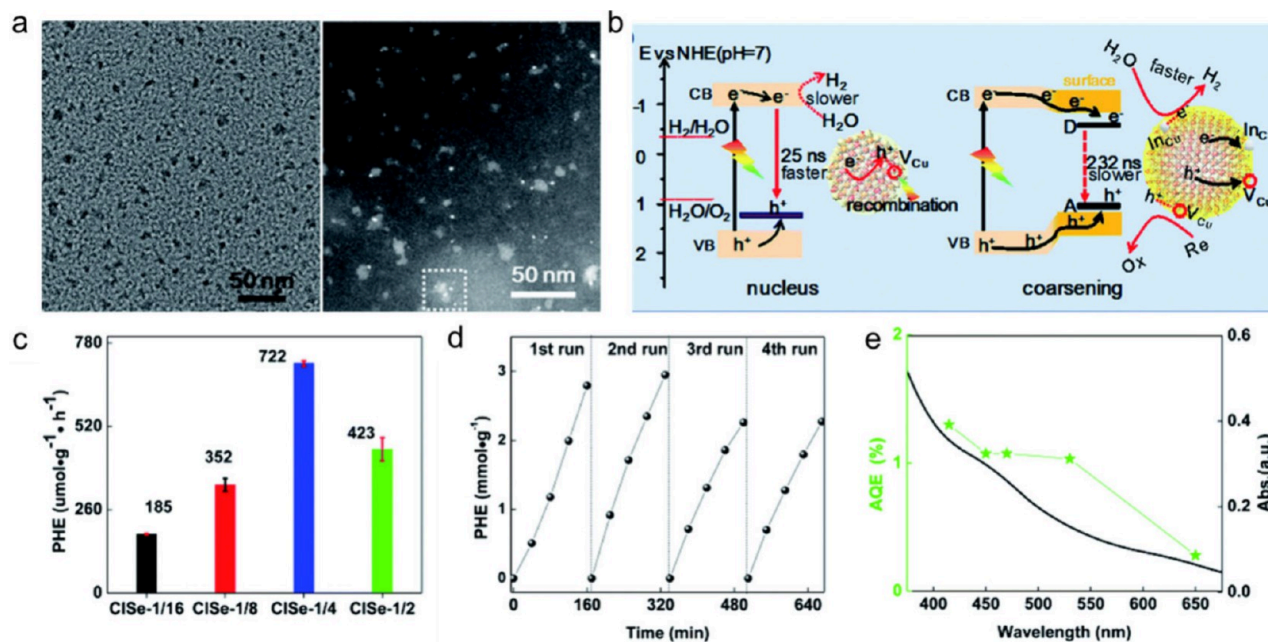

Figure 6. (a) TEM and high-angle annular dark field (HAADF) images of CIS CQDs. (b) Schematic illustration of the photocatalytic H_2 production mechanism. (c) Photocatalytic H_2 evolution performances of CIS CQDs. (d) Cycling stability test of CISe-1/4 for photocatalytic H_2 production. (e) UV−vis absorption spectra and AQE of CISe-1/4 CQDs.[108] Reproduced with permission from ref 108. Copyright 2021 Royal Society of Chemistry.

been made in the fabrication process of QD photoanodes (morphology control, metal doping, core−shell structure, etc.) to develop the applicability of I−III−VI CQDs for PEC and explore the material design principles for efficient PEC H_2 generation.[96−98] Note that defect engineering is also an efficient method to modulate the electrical and photophysical properties of semiconductor materials.[99−101] Furthermore, this method is particularly useful for multinary semiconductors, as they have different types of point defects.

Yang and coauthors reported the defect engineering of CIS CQDs for PEC H_2 production by tuning the reactivity of metal

precursors during the QD synthesis process.[90] CIS CQDs with different In/Cu ratios maintaining their shape and size have been synthesized and employed to sensitize mesoporous TiO_2 films for the fabrication of QD-sensitized photoanodes (Figure 5a). The CIS CQDs with an In/Cu ratio of 1.55 (CIS 3 QDs) possessed the longest carrier lifetime and highest carrier concentration among all the obtained CQDs. Thus, the photoanode fabricated by CIS 3 CQDs generated a champion photocurrent density of 10.7 mA cm^{-2} at 0.6 V vs RHE and a high applied bias photon-to-current efficiency (ABPE) (Figure 5b,c). Besides, the photoanode fabricated by CIS 3 CQDs
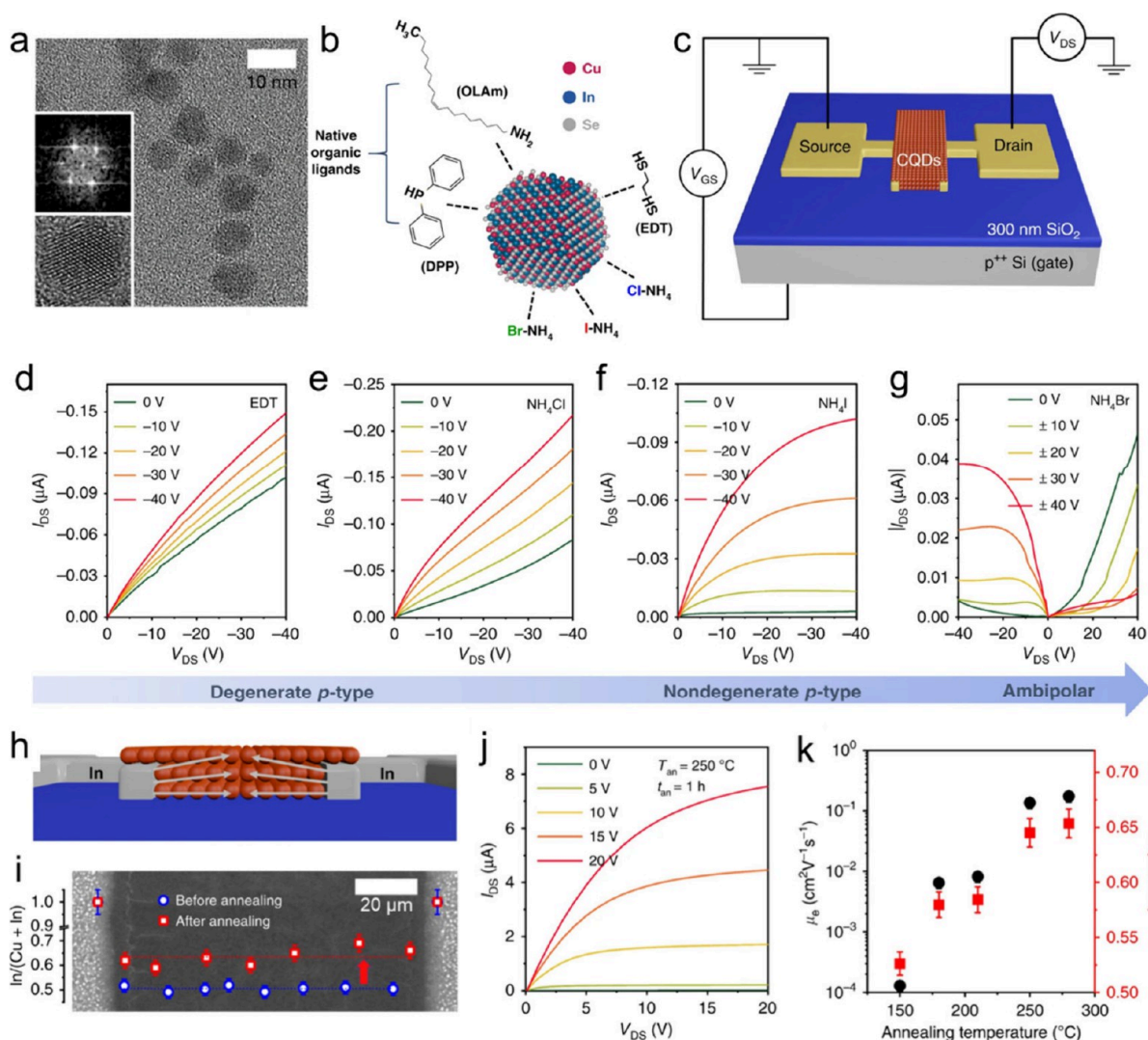
Figure 7. (a) TEM and HRTEM images of CIS CQDs. (b) Schematic illustration of a CIS CQD with different types of capping ligands. (c) Schematic illustration of a p-channel CQD-field-effect transistor (FET). (c–g) Output characteristics of Au-contact p-channel FETs fabricated by colloidal CIS QDs capped with EDT, NH_4Cl, NH_4I, and NH_4Br, respectively. (h,i) Schematic illustration and a top-view SEM image of an In-contact n-channel CIS CQD FET. (j) Output characteristics of In-contact n-channel CIS CQD FETs. (k) Annealing temperature dependent $In/(In + Cu)$ ratio (red squares) and electron mobility (black circles) of an In-contact n-channel CIS CQD FET.[18] Reproduced with permission from ref 18. Copyright 2020 Springer Nature.

exhibited the highest IPCE values over the entire spectral range (Figure 5d). This excellent performance is attributed to the higher electron collection and injection efficiencies compared with other samples.[102] They also investigated the actual H_2 generation performances of photoanodes fabricated by CIS 3 CQDs at 0.6 V vs RHE for 4 h (Figure 5e). The Faradaic efficiency was above 90%, illustrating that most of the measured current during the PEC reaction is used for hydrogen production (Figure 5e). The defect engineering of CIS CQDs can effectively boost the PEC H_2 generation property of CIS QD-sensitized photoanodes.

2.5. Photocatalytic H_2 Production. Photocatalytic water splitting to hydrogen production is an ideal approach for solar-to-hydrogen conversion without byproducts and pollution. I–III–VI CQDs have been widely used for photocatalytic H_2 production due to their Cd-free composition, composition-dependent band structure, multiple photon absorption, size-related photoelectric properties, and unique defect toler-ance.[103−105] CIS among these I−III−VI CQDs has garnered

more attention for photocatalytic H_2 production due to its large exciton Bohr radius (approximately 10.6 nm), which facilitates the regulation of the bandgaps from ultraviolet to the near-infrared region via size.[106,107] More importantly, the defect tolerance and composition-dependent bandgap of CIS CQDs offer an opportunity to enhance the photocatalytic H_2 evolution property through defect engineering.

Yuan and coauthors developed a ligand-assisted two-step aqueous method to synthesize defect CIS CQDs for the first time (Figure 6a).[108] The copper vacancy defects and the substitution of indium at copper site defects obviously changed the absorption properties of the CIS CQDs. The obtained CIS CQDs can effectively catalyze the photocatalytic water splitting process to produce H_2 (Figure 6b). The CIS CQDs exhibited a Cu/In ratio dependent photocatalytic H_2 production property with a champion evolution rate of 722 $\mu mol\ g^{-1}\ h^{-1}$, which is about 23 times higher than that (31 $\mu mol\ g^{-1}\ h^{-1}$) of the initially synthesized CIS nucleus (Figure 6c). Furthermore, the hydro-gen generation rate exhibited no significant decline and
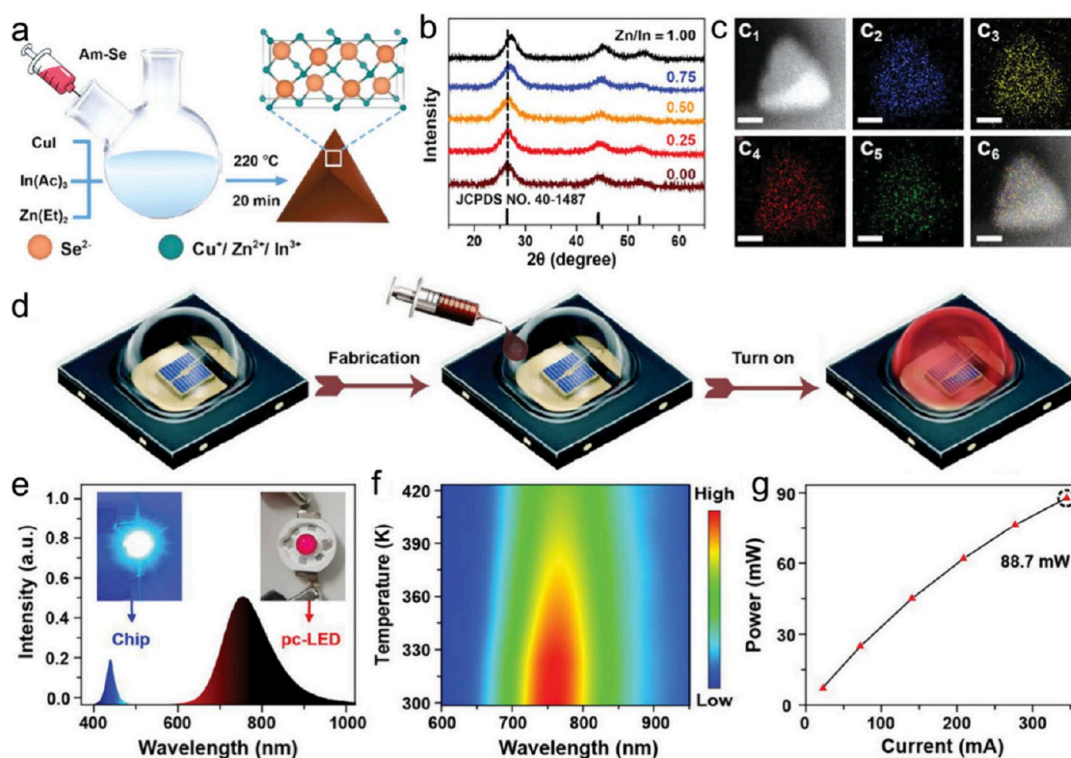
Figure 8. (a) Schematic graph showing the colloidal synthesis of Zn^{2+} doped CIS (CIS-Zn) CQDs. (b) XRD patterns of CIS CQDs with different doping concentrations of Zn^{2+}. (c) EDS-mapping of CIS-Zn CQDs. (d) Schematic illustration of the fabrication of pc-LEDs using CIS-Zn@ZnSe CQDs. (e) Electroluminescence performances of the fabricated pc-LED at an actuation current of 120 mA. (f) Temperature-dependent PL emission properties (λ_{ex} = 365 nm) of the fabricated pc-LED at temperatures from 298 to 423 K. (g) Output power of the fabricated pc-LED at different actuation currents.[23] Reproduced with permission from ref 23. Copyright 2023 Wiley.

consistently maintained above 80% of the initial cycle for CISe-1/4 QDs after four consecutive cycles (Figure 6d). The most efficient CIS CQDs showed a wavelength-dependent AQE of H_2 production with a consistent tendency in the absorption spectrum (Figure 6e) with a maximum AQE of 1.3%.

2.6. QD Transistors. Thin-film transistors (TFTs) and the corresponding integrated circuits have attracted significant attention because they are the fundamental building blocks for fabricating next-generation electronic devices.[109,110] The fabrication of devices on flexible substrates using the widely employed single-crystal and polycrystalline silicon TFT technology is challenging due to the requirement for high process temperatures.[111] In addition, scale-up production of industrial silicon ineluctably leads to high cost and energy consumption.[112] In the last few decades, many semiconductor materials have been studied for replacing silicon to fabricate next-generation electronic devices, such as carbon materials, metal oxides, transition metal chalcogenides, and organic materials.[113−116] The emerging technology of CQD electronics offers an opportunity for combining the advantages of well-understood inorganic semiconductors with solution process-ability.

CQDs are considered as some of the most promising alternatives for silicon due to their high chemical and environmentalal stability and shape-, size-, and composition-controlled electronic properties.[117−119] The CQDs are usually synthesized through a colloidal approach, enabling low-cost fabrication of thin-film electronic devices via easily scalable solution-based methods.[17,30,120] However, the basic and applied research conducted on CQDs is primarily focused on Pb and Cd chalcogenides, which contain highly toxic components that

greatly limit their potential applications.[121−123] I−III−VI$_2$ CQDs are the possible nontoxic alternatives for Pb and Cd chalcogenide QDs and have been widely used for fabricating electronic devices in the fields of transistors, LEDs, and solar energy conversion.[124−126] As an outstanding alternative, CIS CQDs with desirable carrier type, concentration, and mobility can be easily obtained via regulating their size, shape, and composition.[127] In recent years, CIS CQDs have been extensively utilized to fabricate solution-processed TFTs.[30,128,129]

Yuan and coauthors fabricated both *n*- and *p*-channel transistors and the corresponding integrated circuits using CIS CQDs.[18] First, they synthesized highly crystalline CIS CQDs with organic capping ligands by a single-pot colloidal synthesis method (Figure 7a,b). Then, they fabricated *p*-channel FETs with gold drain and source electrodes (Figure 7c) in order to study the hole transport properties of CIS CQD films. Because the synthesized CIS CQDs are overcoated with a shell of organic ligands, the CIS CQD films show a low hole mobility of 2.6×10^{-5} cm^2 V^{-1} s^{-1}, which is attributed to the wide interdot spacing constrained by the long organic ligands. In order to improve the carrier mobilities in CIS CQD films, the original long organic ligands are generally replaced with shorter species, such as 1,2-ethanedithiol (EDT) and halide ligands (e.g., NH_4Cl, NH_4Br and NH_4I).[130−132] The hole mobility increased to ca. 1.3×10^{-4} cm^2 V^{-1} s^{-1} (Figure 7d) when the CIS CQD films were treated with EDT. Similarly, the carrier mobility of CIS CQD films increased by a factor of ca. 10 when they were treated with halide ligands (Figure 7e−g).

Subsequently, they fabricated *n*-channel CIS CQD FETs with indium source and drain contact devices by thermal annealing to
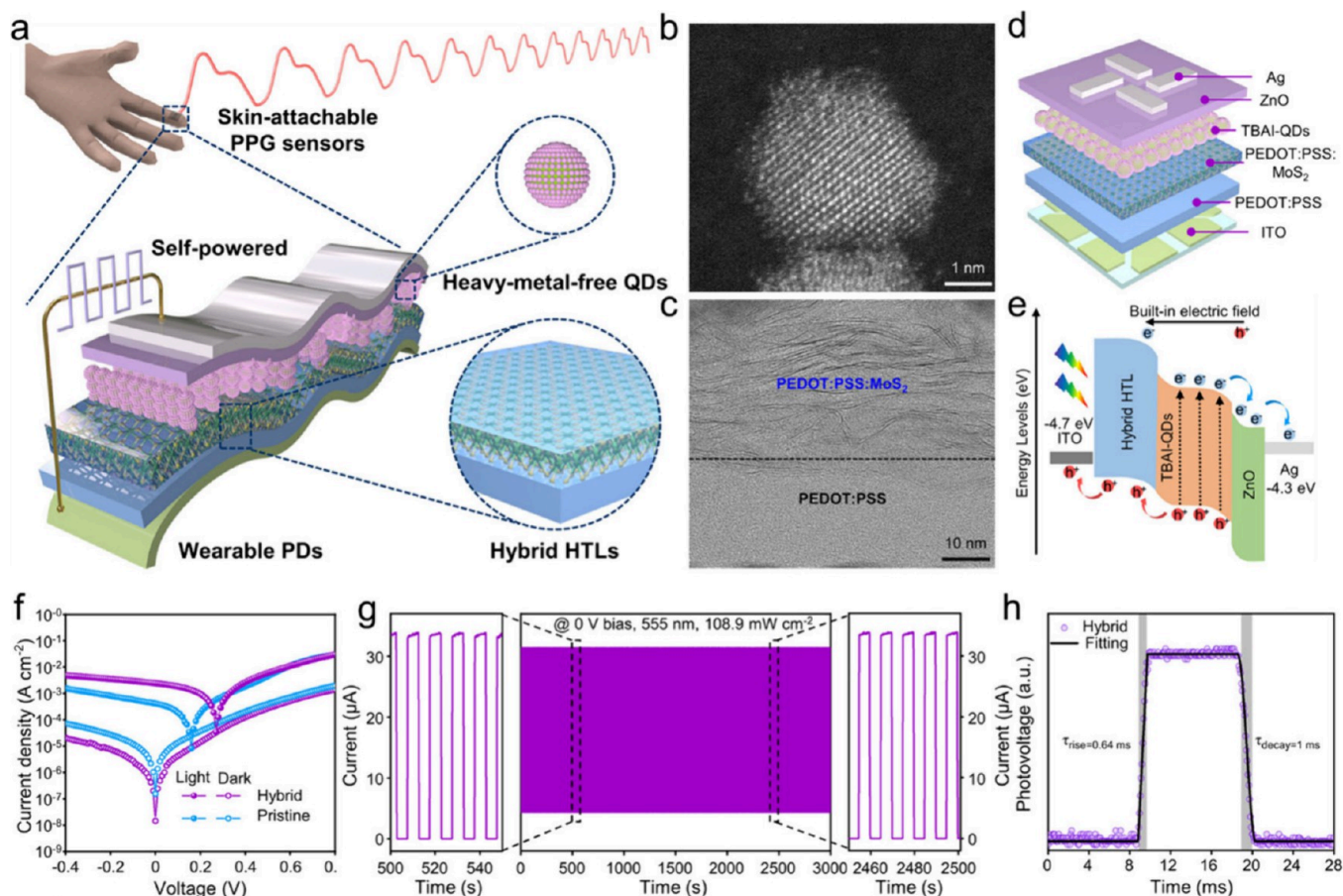
Figure 9. (a) Schematic illustration of ultrathin CIS QD photodetectors. (b,c) STEM image of CIS CQDs and cross-sectional TEM image of the hybrid PEDOT/PSS/MoS$_2$ hole transport layer. (d,e) Schematic and energy level diagrams of the CIS QD photodetectors. (f) $J-V$ measurements of the photodetectors with pristine and hybrid hole transport layers under illumination (555 nm, 91.7 mW cm^{-2}) and in the dark. (g) Time-dependent photoresponse of the hybrid photodetectors at 0 V bias under illumination (555 nm, 108.9 mW cm^{-2}). (h) Rise and decay times of the hybrid photodetectors.[28] Reproduced with permission from ref 28. Copyright 2023 American Chemical Society.

study the electron transport property of CIS CQD films (Figure 7h,i). The annealed In-contact FET fabricated by NH$_4$I-treated CIS CQDs exhibited an excellent *n*-type property with an electron mobility of ca. 0.14 cm^2 V^{-1} s^{-1} (Figure 7j). Interestingly, the electron mobility (black circles) rapidly increased with the annealing temperature, which was related to the increase of the In ratio in the CQDs (Figure 7k). Importantly, the integrated logic circuits made of *p*- and *n*-channel CIS CQD FETs show low switching voltages compatible with standard complementary metal-oxide-semiconductor devices.

2.7. QD LEDs. Semiconductor QDs serve as a class of widely known light-emitting nanocrystals, which have been used as efficient lighting materials for decades.[133−135] Although the common CdSe CQDs have serious environmental issues, such as toxicity, they are widely used lighting materials in commercial LEDs.[136−138] Many efforts have been made to find environmentally benign QDs to replace Cd-based QDs for commercial applications. I−III−VI ternary CQDs are promising alternatives for lighting applications due to their green and environmental friendliness, high emission intensity, and tunable PL emission ranges from the visible to NIR window.[126,139−141] Furthermore, strong and stable luminescence is important for practical applications.

CIS with a narrow bandgap of 1.04 eV and a large exciton Bohr radius of ca. 10.6 nm is predicted to be a promising

luminescent emitter in the red and near-infrared light region.[15,127,142] Allen and coauthor successfully synthesized CIS CQDs with a remarkable photoluminescence quantum yield (PLQY) of 25%.[143] Nose and coauthors have obtained stoichiometric CIS CQDs with PLQYs of 5%, later improving the PLQYs to 16% through coating a ZnSe shell on CIS QDs.[144] Subsequently, several researchers have successfully improved the PLQYs through shell engineering. Cassette and coauthors synthesized CIS/ZnS core/shell CQDs with PLQYs up to 50%.[145] Park and coauthors produced In-rich CIS CQDs with PLQYs of 20−30%, improving the PL efficiency up to 60% via ZnS-shell protection.[146] The excellent NIR PL emission property of CIS CQDs makes them an ideal choice as a luminescent material for portable mini- or microphosphor-converted LEDs (pc-LEDs).

Chen and coauthors reported the design of broad-band NIR CIS CQDs for micro pc-LED applications. High-quality Zn^{2+} doped CIS CQDs were prepared through a hot-injection method (Figure 8a).[23] The PL emission peak was manipulated from 855 to 1150 nm by adjusting the Cu/In ratios. Moreover, the Zn dopant has a nearly negligible influence on the crystal structure of CIS CQDs (Figure 8b) and is homogeneously distributed throughout the CISe-Zn CQD (Figure 8c). Furthermore, the PLQY of CISe-Zn CQD could be improved from 28.6% to 92.8% through coating a ZnSe shell. Subsequently, they fabricated a NIR pc-LED using CISe-Zn@

ZnSe CQDs as phosphors combined with a commercial blue chip (Figure 8d). The fabricated NIR pc-LED shows a broad NIR emission in the region of 600−1000 nm (CISe-Zn@ZnSe CQDs) and a blue emission at 450 nm (chip) (Figure 8e). Importantly, the fabricated NIR pc-LED exhibited good thermal stability at temperatures from 298 to 423 K (Figure 8f). The output power increased with the actuation current and a high NIR output power of 88.7 mW could be achieved at an actuation current of 350 mA (Figure 8g), which is much higher than those of the reported Cd/Pb-free QD-based NIR pc-LEDs.[147−149]

2.8. QD Photodetectors. Photodetectors which can convert different photons into electrical signals are widely utilized in optical communications, light cameras, and medicine.[150−152] Till now, many semiconductor materials have been used as photoactive layers in photodetectors, such as silicon, QDs, transition metal chalcogenides, and conjugated polymers.[153−156] However, they always have a high cost and require a complicated fabrication process.[157] Solution-processed CQDs with quantum size effect tuning are compatible with a series of substrates, enabling a direct integration with commercial microelectronics, microfluidics, organic circuits, and optical circuitry.[5,158−160] Many solution-processed CQD ultrasensitive photodetectors have been demonstrated in both the visible and infrared region, but these devices are usually fabricated by using toxic Cd/Pb-based QDs.[161,162] The exploration of environmentally friendly QDs to achieve high detectivity in photodetectors is still required.

Recently, heavy-metal-free CIS nanomaterials with different shapes have attracted attention as a key material for application in ecofriendly photodetectors owing to their direct bandgap transient characteristics, stable phase structure, wide absorption range covering the ultraviolet to near-infrared region, and nontoxicity.[25,163−165] Li and coauthors used heavy-metal-free CIS CQDs to fabricate ultrathin self-powered photodetectors, which enable high-performance wearable photoplethysmography-based health monitoring systems (Figure 9a).[28] CIS CQDs capped with I$^-$ were used to fabricate ultrathin light absorption layers (∼40 nm); mixtures of p-type colloidal MoS_2 nanosheets and poly(3,4-ethylenedioxythiophene):poly(styrenesulfonate) (PEDOT:PSS) were employed as hole transport layers (HTLs), and n-type ZnO nanoparticles were used as electron transport layers (ETLs) (Figure 9b,c).

Ultrathin CIS QD photodetectors are fabricated in a structure with ITO/HTL (60 nm)/TBAI-QDs (40 nm)/ZnO (23 nm)/ Ag (90 nm) (Figure 9d). The energy band of CIS QDs is situated between those of the ZnO and HTL, driving photogenerated holes and electrons across the interface to reach the ITO and Ag electrodes, respectively (Figure 9e). Figure 9f shows the $J-V$ curves of pristine photodetectors fabricated with pure PEDOT:PSS and hybrid photodetectors fabricated with hybrid HTLs, which were recorded under 555 nm illumination (91.7 mW cm^{-2}) and in the dark. The dark-current and photocurrent densities of the hybrid photodetectors are more than 10-fold lower and 5-fold higher than those of the pristine photodetectors at 0 V bias, respectively. These excellent performances are attributed to the rapid charge extraction realized by hybrid HTLs and restrained charge injection via a strong potential barrier coming from enhanced photovoltage. The hybrid photodetectors exhibited a reversible and stable I_{light}/I_{dark} ratio of ∼8.6×10^4 under periodic switching at 555 nm without degradation after 3000 s of continuous operation, illustrating the excellent photostability (Figure 9g). In addition, both the rise and decay times of the hybrid photodetectors are

shorter than those of the pristine photodetectors (Figure 9h). Moreover, the CIS QD photodetectors can be integrated into skin-attachable photoplethysmography sensors for accurate real-time healthcare monitoring.

3. SUMMARY AND PERSPECTIVES

Recently, there has been significant progress in the development of CIS CQDs due to their strong light absorption and bright emission in both visible and infrared regions, large Stokes shift, and relatively lower toxicity compared to conventional CdX and PbX (X = S, Se, and Te) QDs. The composition-dependent bandgap and special defect tolerance of CIS CQDs enable convenient customization of band alignment for various applications, making them highly suitable for solar energy conversion, displays, and electronic devices. This review presents a comprehensive overview of recent optical applications involving CIS CQDs, including QD solar cells, QDSSCs, and QD LSCs. Additionally, it discusses the utilization of these materials in photocatalytic and photoelectrochemical H_2 production, QD transistors, QD LEDs, and QD photodetectors. Although significant progress has been achieved in the optical applications of CIS CQDs, several unresolved challenges necessitate further investigations into their device applications. Herein, we provide insights into current challenges and offer suggestions for future advancements.

(1) The large-scale synthesis of CIS CQDs is fundamental for commercialization. Achieving gram-scale synthesis of CIS CQDs without compromising quality remains a significant challenge, and there is an urgent need to design reactions beyond the laboratory scale. Additionally, the lack of precise control over size and composition hinders the investigation of their size- and composition-dependent optical properties.

(2) The future device applications based on CIS CQDs are typically fabricated using printing techniques. Therefore, it is essential to modulate the surface of CIS CQDs with suitable ligands, enabling their effective dispersion in various solvents. Consequently, ligands consisting of short-chain organic compounds that exhibit stability at high temperatures are highly preferred.

(3) Although significant progress has been made in CIS QD-based devices, their performance still falls short of practical applications. The understanding of the working mechanism and the design of more device structures are essential for advancing the functionality of the devices. Taking the QD photodetectors for example, the performances can be enhanced by optimizing the design of better electron and hole transport layers.

■ AUTHOR INFORMATION

Corresponding Author

   Liang Wu − *School of Chemistry and Materials Science, Anhui Normal University, Wuhu 241002, People's Republic of China;* ● orcid.org/0009-0003-2377-093X; Email: wuliang@ahnu.edu.cn

Authors

   Song Chen − *School of Chemistry and Materials Science, Anhui Normal University, Wuhu 241002, People's Republic of China*

Bingqian Zu − *School of Chemistry and Materials Science, Anhui Normal University, Wuhu 241002, People's Republic of China*

Complete contact information is available at:
https://pubs.acs.org/10.1021/acsomega.4c03802

Notes
The authors declare no competing financial interest.

■ ACKNOWLEDGMENTS

■ ABBREVIATIONS

QDs, quantum dots; CIS, CuInSe$_2$; DOS, density of state; CQDs, colloidal quantum dots; PEC, photoelectrochemical; QDSSCs, quantum dot sensitized solar cells; LSCs, luminescence solar concentrators; LEDs, light-emitting diodes; EQE, external quantum efficiency; PCE, power conversion effciency; AQE, apparent quantum efficiency; HAADF, high-angle annular dark field; TFTs, thin-film transistors; PLQYs, photoluminescence quantum yields; PL, photoluminescence; NIR, near-infrared; HTLs, hole transport layers; ETLs, electron transport layers

■ REFERENCES

(1) Fan, F.; Voznyy, O.; Sabatini, R. P.; Bicanic, K. T.; Adachi, M. M.; McBride, J. R.; Reid, K. R.; Park, Y. S.; Li, X.; Jain, A.; Quintero-Bermudez, R.; Saravanapavanantham, M.; Liu, M.; Korkusinski, M.; Hawrylak, P.; Klimov, V. I.; Rosenthal, S. J.; Hoogland, S.; Sargent, E. H. Continuous-wave lasing in colloidal quantum dot solids enabled by facet-selective epitaxy. *Nature* **2017**, *544* (7648), 75−79.

(2) Mokari, T.; et al. Selective Growth of Metal Tips onto Semiconductor Quantum Rods and Tetrapods. *Science* **2004**, *304* (5678), 1787−1790.

(3) Hou, J.; Li, W.; Zhang, H.; Sidhik, S.; Fletcher, J.; Metcalf, I.; Anantharaman, S. B.; Shuai, X.; Mishra, A.; Blancon, J.-C.; Katan, C.; Jariwala, D.; Even, J.; Kanatzidis, M. G.; Mohite, A. D. Synthesis of 2D perovskite crystals via progressive transformation of quantum well thickness. *Nat. Synth.* **2024**, *3* (2), 265−275.

(4) García de Arquer, F. P.; Talapin, D. V.; Klimov, V. I.; Arakawa, Y.; Bayer, M.; Sargent, E. H. Semiconductor quantum dots: Technological progress and future challenges. *Science* **2021**, *373* (6555), No. eaaz8541.

(5) Kagan, C. R.; Lifshitz, E.; Sargent, E. H.; Talapin, D. V. Building devices from colloidal quantum dots. *Science* **2016**, *353* (6302), aac5523.

(6) Mocatta, D.; Cohen, G.; Schattner, J.; Millo, O.; Rabani, E.; Banin, U. Heavily doped semiconductor nanocrystal quantum dots. *Science* **2011**, *332* (6025), 77−81.

(7) Won, Y.-H.; Cho, O.; Kim, T.; Chung, D.-Y.; Kim, T.; Chung, H.; Jang, H.; Lee, J.; Kim, D.; Jang, E. Highly efficient and stable InP/ZnSe/ZnS quantum dot light-emitting diodes. *Nature* **2019**, *575* (7784), 634−638.

(8) Klimov, V. I. Multicarrier Interactions in Semiconductor Nanocrystals in Relation to the Phenomena of Auger Recombination and Carrier Multiplication. *Annu. Rev. Conden. Ma. P.* **2014**, *5* (1), 285−316.

(9) Rossetti, R.; Nakahara, S.; Brus, L. E. Quantum size effects in the redox potentials, resonance Raman spectra, and electronic spectra of CdS crystallites in aqueous solution. *J. Chem. Phys.* **1983**, *79* (2), 1086−1088.

(10) Ossia, Y.; Levi, A.; Panfil, Y. E.; Koley, S.; Scharf, E.; Chefetz, N.; Remennik, S.; Vakahi, A.; Banin, U. Electric-field-induced colour switching in colloidal quantum dot molecules at room temperature. *Nat. Mater.* **2023**, *22* (10), 1210−1217.

(11) Almeida, G.; Ubbink, R. F.; Stam, M.; du Fossé, I.; Houtepen, A. J. InP colloidal quantum dots for visible and near-infrared photonics. *Nat. Rev. Mater.* **2023**, *8* (11), 742−758.

(12) Wang, Y.; Kavanagh, S. R.; Burgués-Ceballos, I.; Walsh, A.; Scanlon, D. O.; Konstantatos, G. Cation disorder engineering yields AgBiS2 nanocrystals with enhanced optical absorption for efficient ultrathin solar cells. *Nat. Photonics* **2022**, *16* (3), 235−241.

(13) Liang, W. F.; Nie, C. M.; Du, J.; Han, Y. Y.; Zhao, G. H.; Yang, F.; Liang, G. J.; Wu, K. F. Near-infrared photon upconversion and solar synthesis using lead-free nanocrystals. *Nat. Photonics* **2023**, *17* (4), 346−357.

(14) Lox, J. F. L.; Dang, Z.; Dzhagan, V. M.; Spittel, D.; Martín-García, B.; Moreels, I.; Zahn, D. R. T.; Lesnyak, V. Near-Infrared Cu-In-Se-Based Colloidal Nanocrystals via Cation Exchange. *Chem. Mater.* **2018**, *30* (8), 2607−2617.

(15) Yarema, O.; Bozyigit, D.; Rousseau, I.; Nowack, L.; Yarema, M.; Heiss, W.; Wood, V. Highly Luminescent, Size- and Shape-Tunable Copper Indium Selenide Based Colloidal Nanocrystals. *Chem. Mater.* **2013**, *25* (18), 3753−3757.

(16) Harvey, S. M.; Houck, D. W.; Kirschner, M. S.; Flanders, N. C.; Brumberg, A.; Leonard, A. A.; Watkins, N. E.; Chen, L. X.; Dichtel, W. R.; Zhang, X.; Korgel, B. A.; Wasielewski, M. R.; Schaller, R. D. Transient Lattice Response upon Photoexcitation in CuInSe2 Nanocrystals with Organic or Inorganic Surface Passivation. *ACS Nano* **2020**, *14* (10), 13548−13556.

(17) Guo, R. Q.; Zhang, L. X.; Meng, J.; Liu, A. Q.; Yuan, J. F.; Zheng, K. B.; Tian, J. J. Exploiting Flexible Memristors Based on Solution-Processed Colloidal CuInSe Nanocrystals. *Adv. Electron. Mater.* **2020**, *6* (5), 2000035.

(18) Yun, H. J.; Lim, J.; Roh, J.; Neo, D. C. J.; Law, M.; Klimov, V. I. Solution-processable integrated CMOS circuits based on colloidal CuInSe2 quantum dots. *Nat. Commun.* **2020**, *11* (1), 5280.

(19) Du, J.; Singh, R.; Fedin, I.; Fuhr, A. S.; Klimov, V. I. Spectroscopic insights into high defect tolerance of Zn:CuInSe2 quantum-dot-sensitized solar cells. *Nat. Energy* **2020**, *5* (5), 409−417.

(20) de Kergommeaux, A.; Fiore, A.; Bruyant, N.; Chandezon, F.; Reiss, P.; Pron, A.; de Bettignies, R.; Faure-Vincent, J. Synthesis of colloidal CuInSe2 nanocrystals films for photovoltaic applications. *Sol. Energy Mater. Sol. Cells* **2011**, *95* (Supplement1), S39−S43.

(21) Liu, W.; Turkani, V. S.; Akhavan, V.; Korgel, B. A. Photonic Lift-off Process to Fabricate Ultrathin Flexible Solar Cells. *ACS Appl. Mater. Interfaces* **2021**, *13* (37), 44549−44555.

(22) Houck, D. W.; Siegler, T. D.; Korgel, B. A. Predictive Modeling of CuInSe2 Nanocrystal Photovoltaics: The Importance of Band Alignment and Carrier Diffusion. *ACS Appl. Energy Mater.* **2019**, *2* (2), 1494−1504.

(23) Lian, W.; Tu, D.; Weng, X.; Yang, K.; Li, F.; Huang, D.; Zhu, H.; Xie, Z.; Chen, X. Near-Infrared Nanophosphors Based on CuInSe2 Quantum Dots with Near-Unity Photoluminescence Quantum Yield for Micro-LEDs Applications. *Adv. Mater.* **2024**, *36* (9), 2311011.

(24) McDaniel, H.; Fuke, N.; Pietryga, J. M.; Klimov, V. I. Engineered CuInSexS2-x Quantum Dots for Sensitized Solar Cells. *J. Phys. Chem. Lett.* **2013**, *4* (3), 355−361.

(25) Wang, J.-J.; Wang, Y.-Q.; Cao, F.-F.; Guo, Y.-G.; Wan, L.-J. Synthesis of Monodispersed Wurtzite Structure CuInSe2 Nanocrystals and Their Application in High-Performance Organic- Inorganic Hybrid Photodetectors. *J. Am. Chem. Soc.* **2010**, *132* (35), 12218−12221.

(26) Kim, M. R.; Ma, D. Quantum-Dot-Based Solar Cells: Recent Advances, Strategies, and Challenges. *J. Phys. Chem. Lett.* **2015**, *6* (1), 85−99.

(27) Tian, J.; Cao, G. Semiconductor quantum dot-sensitized solar cells. *Nano Rev.* **2013**, *4* (1), 22578.

(28) Li, S.; Jang, J. H.; Chung, W.; Seung, H.; Park, S. I.; Ma, H.; Pyo, W. J.; Choi, C.; Chung, D. S.; Kim, D.-H.; Choi, M. K.; Yang, J. Ultrathin Self-Powered Heavy-Metal-Free Cu-In-Se Quantum Dot Photodetectors for Wearable Health Monitoring. *ACS Nano* **2023**, *17* (20), 20013−20023.

(29) Li, F.; Guo, C.; Pan, R.; Zhu, Y.; You, L.; Wang, J.; Jin, X.; Zhang, Q.; Song, Y.; Chen, Z.; Li, Q. Integration of green CuInS2/ZnS quantum dots for high-efficiency light-emitting diodes and high-responsivity photodetectors. *Opt. Mater. Express* **2018**, *8* (2), 314−323.

(30) Pang, C.; Hu, S. B.; Guo, C.; Wang, J. T.; Zou, S. H.; Pan, Z. X.; Liu, J. C.; Shen, L. M.; Bao, N. Z.; Ning, H. L.; Gupta, A.; Gong, Z. High-Performance Inorganically Connected CuInSe Nanocrystal Thin-Film Transistors and Integrated Circuits Based on the Solution Process of Colloidal Synthesis, Ligand Exchange, and Surface Treatment. *Chem. Mater.* **2021**, *33* (22), 8775−8785.

(31) Lewis, N. S. Research opportunities to advance solar energy utilization. *Science* **2016**, *351* (6271), aad1920.

(32) Chen, S.; Takata, T.; Domen, K. Particulate photocatalysts for overall water splitting. *Nat. Rev. Mater.* **2017**, *2*, 17050.

(33) Meinardi, F.; Ehrenberg, S.; Dhamo, L.; Carulli, F.; Mauri, M.; Bruni, F.; Simonutti, R.; Kortshagen, U.; Brovelli, S. Highly efficient luminescent solar concentrators based on earth-abundant indirect-bandgap silicon quantum dots. *Nat. Photonics* **2017**, *11* (3), 177−185.

(34) Zhao, Q.; Han, R.; Marshall, A. R.; Wang, S.; Wieliczka, B. M.; Ni, J.; Zhang, J. J.; Yuan, J. Y.; Luther, J. M.; Hazarika, A.; Li, G. R. Colloidal Quantum Dot Solar Cells: Progressive Deposition Techniques and Future Prospects on Large-Area Fabrication. *Adv. Mater.* **2022**, *34* (17), 2107888.

(35) Kramer, I. J.; Sargent, E. H. The architecture of colloidal quantum dot solar cells: materials to devices. *Chem. Rev.* **2014**, *114* (1), 863−82.

(36) Carey, G. H.; Abdelhady, A. L.; Ning, Z.; Thon, S. M.; Bakr, O. M.; Sargent, E. H. Colloidal Quantum Dot Solar Cells. *Chem. Rev.* **2015**, *115* (23), 12732−12763.

(37) Gur, I.; Fromer, N. A.; Geier, M. L.; Alivisatos, A. P. Air-Stable All-Inorganic Nanocrystal Solar Cells Processed from Solution. *Science* **2005**, *310* (5747), 462−465.

(38) Yuan, M.; Liu, M.; Sargent, E. H. Colloidal quantum dot solids for solution-processed solar cells. *Nat. Energy* **2016**, *1* (3), 16016.

(39) Zhao, H.; Rosei, F. Colloidal Quantum Dots for Solar Technologies. *Chem.* **2017**, *3* (2), 229−258.

(40) Vidal, R.; Alberola-Borràs, J. A.; Habisreutinger, S. N.; Gimeno-Molina, J. L.; Moore, D. T.; Schloemer, T. H.; Mora-Seró, I.; Berry, J. J.; Luther, J. M. Assessing health and environmental impacts of solvents for producing perovskite solar cells. *Nat. Sustain.* **2021**, *4* (3), 277−285.

(41) Bernechea, M.; Miller, N. C.; Xercavins, G.; So, D.; Stavrinadis, A.; Konstantatos, G. Solution-processed solar cells based on environmentally friendly AgBiS2 nanocrystals. *Nat. Photonics* **2016**, *10* (8), 521−525.

(42) Panthani, M. G.; Stolle, C. J.; Reid, D. K.; Rhee, D. J.; Harvey, T. B.; Akhavan, V. A.; Yu, Y.; Korgel, B. A. CuInSe2Quantum Dot Solar Cells with High Open-Circuit Voltage. *J. Phys. Chem. Lett.* **2013**, *4* (12), 2030−2034.

(43) Stolle, C. J.; Harvey, T. B.; Pernik, D. R.; Hibbert, J. I.; Du, J.; Rhee, D. J.; Akhavan, V. A.; Schaller, R. D.; Korgel, B. A. Multiexciton Solar Cells of CuInSe2 Nanocrystals. *J. Phys. Chem. Lett.* **2014**, *5* (2), 304−309.

(44) Pietryga, J. M.; Park, Y.-S.; Lim, J.; Fidler, A. F.; Bae, W. K.; Brovelli, S.; Klimov, V. I. Spectroscopic and Device Aspects of Nanocrystal Quantum Dots. *Chem. Rev.* **2016**, *116* (18), 10513−10622.

(45) Jackson, P.; Hariskos, D.; Lotter, E.; Paetel, S.; Wuerz, R.; Menner, R.; Wischmann, W.; Powalla, M. New world record efficiency for Cu(In,Ga)Se2 thin-film solar cells beyond 20%. *Prog. Photovoltaics Res. Appl.* **2011**, *19* (7), 894−897.

(46) Stolle, C. J.; Panthani, M. G.; Harvey, T. B.; Akhavan, V. A.; Korgel, B. A. Comparison of the Photovoltaic Response of Oleylamine and Inorganic Ligand-Capped CuInSe2 Nanocrystals. *ACS Appl. Mater. Interfaces* **2012**, *4* (5), 2757−2761.

(47) Akhavan, V. A.; Panthani, M. G.; Goodfellow, B. W.; Reid, D. K.; Korgel, B. A. Thickness-limited performance of CuInSe2 nanocrystal photovoltaic devices. *Opt. Express* **2010**, *18* (S3), A411−A420.

(48) Guo, Q.; Ford, G. M.; Agrawal, R.; Hillhouse, H. W. Ink formulation and low-temperature incorporation of sodium to yield 12%
efficient Cu(In,Ga)(S,Se)2 solar cells from sulfide nanocrystal inks. *Prog. Photovoltaics Res. Appl.* **2013**, *21* (1), 64−71.

(49) Wang, Y. X.; Wei, M.; Fan, F. J.; Zhuang, T. T.; Wu, L.; Yu, S. H.; Zhu, C. F. Phase-Selective Synthesis of Cu2ZnSnS4 Nanocrystals through Cation Exchange for Photovoltaic Devices. *Chem. Mater.* **2014**, *26* (19), 5492−5498.

(50) Anand, A.; Zaffalon, M. L.; Gariano, G.; Camellini, A.; Gandini, M.; Brescia, R.; Capitani, C.; Bruni, F.; Pinchetti, V.; Zavelani-Rossi, M.; Meinardi, F.; Crooker, S. A.; Brovelli, S. Evidence for the Band-Edge Exciton of CuInS2 Nanocrystals Enables Record Efficient Large-Area Luminescent Solar Concentrators Nanocrystals Enables Record Efficient Large-Area Luminescent Solar Concentrators. *Adv. Funct. Mater.* **2020**, *30* (4), 1906629.

(51) Meinardi, F.; Colombo, A.; Velizhanin, K. A.; Simonutti, R.; Lorenzon, M.; Beverina, L.; Viswanatha, R.; Klimov, V. I.; Brovelli, S. Large-area luminescent solar concentrators based on 'Stokes-shift-engineered' nanocrystals in a mass-polymerized PMMA matrix. *Nat. Photonics* **2014**, *8*, 392−399.

(52) McKenna, B.; Evans, R. C. Towards Efficient Spectral Converters through Materials Design for Luminescent Solar Devices. *Adv. Mater.* **2017**, *29* (28), 1606491.

(53) Wu, K. F.; Li, H. B.; Klimov, V. I. Tandem luminescent solar concentrators based on engineered quantum dots. *Nat. Photonics* **2018**, *12* (2), 105−110.

(54) Debije, M. Better luminescent solar panels in prospect. *Nature* **2015**, *519* (7543), 298−299.

(55) Meinardi, F.; Bruni, F.; Brovelli, S. Luminescent solar concentrators for building-integrated photovoltaics. *Nat. Rev. Mater.* **2017**, *2*, 17072.

(56) Pritchard, J.; Simon, K.; Dowd, C.; Joshi, E. Solar power concentrators for space applications. *PAM Rev. Energy Sci. Technol.* **2016**, *3*, 2−26.

(57) Cambié, D.; Zhao, F.; Hessel, V.; Debije, M. G.; Noël, T. A Leaf-Inspired Luminescent Solar Concentrator for Energy-Efficient Continuous-Flow Photochemistry. *Angew. Chem., Int. Ed.* **2017**, *56* (4), 1050−1054.

(58) Weber, W. H.; Lambe, J. Luminescent greenhouse collector for solar radiation. *Appl. Opt.* **1976**, *15* (10), 2299−2300.

(59) Batchelder, J. S.; Zewai, A. H.; Cole, T. Luminescent solar concentrators. 1: Theory of operation and techniques for performance evaluation. *Appl. Opt.* **1979**, *18* (18), 3090−3110.

(60) Currie, M. J.; Mapel, J. K.; Heidel, T. D.; Goffri, S.; Baldo, M. A. High-Efficiency Organic Solar Concentrators for Photovoltaics. *Science* **2008**, *321* (5886), 226−228.

(61) Li, H.; Wu, K.; Lim, J.; Song, H.-J.; Klimov, V. I. Doctor-blade deposition of quantum dots onto standard window glass for low-loss large-area luminescent solar concentrators. *Nat. Energy* **2016**, *1*, 16157.

(62) Lim, J.; Park, Y.-S.; Klimov, V. I. Optical gain in colloidal quantum dots achieved with direct-current electrical pumping. *Nat. Mater.* **2018**, *17*, 42−49.

(63) Meinardi, F.; McDaniel, H.; Carulli, F.; Colombo, A.; Velizhanin, K. A.; Makarov, N. S.; Simonutti, R.; Klimov, V. I.; Brovelli, S. Highly efficient large-area colourless luminescent solar concentrators using heavy-metal-free colloidal quantum dots. *Nat. Nanotechnol.* **2015**, *10* (10), 878−885.

(64) Du, J.; Du, Z.; Hu, J.-S.; Pan, Z.; Shen, Q.; Sun, J.; Long, D.; Dong, H.; Sun, L.; Zhong, X.; Wan, L.-J. Zn-Cu-In-Se Quantum Dot Solar Cells with a Certified Power Conversion Efficiency of 11.6%. *J. Am. Chem. Soc.* **2016**, *138* (12), 4201−4209.

(65) Zhao, K.; Pan, Z.; Mora-Seró, I.; Cánovas, E.; Wang, H.; Song, Y.; Gong, X.; Wang, J.; Bonn, M.; Bisquert, J.; Zhong, X. Boosting Power Conversion Efficiencies of Quantum-Dot-Sensitized Solar Cells Beyond 8% by Recombination Control. *J. Am. Chem. Soc.* **2015**, *137* (16), 5602−5609.

(66) Dong, H.; Xu, F.; Sun, Z.; Wu, X.; Zhang, Q.; Zhai, Y.; Tan, X. D.; He, L.; Xu, T.; Zhang, Z.; Duan, X.; Sun, L. In situ interface engineering for probing the limit of quantum dot photovoltaic devices. *Nat. Nanotechnol.* **2019**, *14* (10), 950−956.

(67) O'Regan, B.; Grätzel, M. A low-cost, high-efficiency solar cell based on dye-sensitized colloidal TiO2 films. *Nature* **1991**, *353* (6346), 737−740.

(68) Rasal, A. S.; Yadav, S.; Kashale, A. A.; Altaee, A.; Chang, J.-Y. Stability of quantum dot-sensitized solar cells: A review and prospects. *Nano Energy* **2022**, *94*, 106854.

(69) Tian, J.; Gao, R.; Zhang, Q.; Zhang, S.; Li, Y.; Lan, J.; Qu, X.; Cao, G. Enhanced Performance of CdS/CdSe Quantum Dot Cosensitized Solar Cells via Homogeneous Distribution of Quantum Dots in TiO2 Film. *J. Phys. Chem. C* **2012**, *116* (35), 18655−18662.

(70) Abate, M. A.; Dehvari, K.; Chang, J.-Y.; Waki, K. Aqueous synthesis of Mn-doped CuInSe2 quantum dots to enhance the performance of quantum dot sensitized solar cells. *Dalton Trans.* **2019**, *48* (42), 16115−16122.

(71) Yan, X.; Cui, X.; Li, B.; Li, L.-s. Large, Solution-Processable Graphene Quantum Dots as Light Absorbers for Photovoltaics. *Nano Lett.* **2010**, *10* (5), 1869−1873.

(72) Song, H.; Lin, Y.; Zhou, M.; Rao, H.; Pan, Z.; Zhong, X. Zn-Cu-In-S-Se Quinary "Green" Alloyed Quantum-Dot-Sensitized Solar Cells with a Certified Efficiency of 14.4%. *Angew. Chem., Int. Ed.* **2021**, *60* (11), 6137−6144.

(73) McDaniel, H.; Fuke, N.; Makarov, N. S.; Pietryga, J. M.; Klimov, V. I. An integrated approach to realizing high-performance liquid-junction quantum dot sensitized solar cells. *Nat. Commun.* **2013**, *4* (1), 2887.

(74) Song, H.; Lin, Y.; Zhang, Z.; Rao, H.; Wang, W.; Fang, Y.; Pan, Z.; Zhong, X. Improving the Efficiency of Quantum Dot Sensitized Solar Cells beyond 15% via Secondary Deposition. *J. Am. Chem. Soc.* **2021**, *143* (12), 4790−4800.

(75) Pan, Z.; Yue, L.; Rao, H.; Zhang, J.; Zhong, X.; Zhu, Z.; Jen, A. K. Y. Boosting the Performance of Environmentally Friendly Quantum Dot-Sensitized Solar Cells over 13% Efficiency by Dual Sensitizers with Cascade Energy Structure. *Adv. Mater.* **2019**, *31* (49), 1903696.

(76) Wang, W.; Zhao, L.; Wang, Y.; Xue, W.; He, F.; Xie, Y.; Li, Y. Facile Secondary Deposition for Improving Quantum Dot Loading in Fabricating Quantum Dot Solar Cells. *J. Am. Chem. Soc.* **2019**, *141* (10), 4300−4307.

(77) Kim, J.-Y.; Yang, J.; Yu, J. H.; Baek, W.; Lee, C.-H.; Son, H. J.; Hyeon, T.; Ko, M. J. Highly Efficient Copper-Indium-Selenide Quantum Dot Solar Cells: Suppression of Carrier Recombination by Controlled ZnS Overlayers. *ACS Nano* **2015**, *9* (11), 11286−11295.

(78) Jara, D. H.; Yoon, S. J.; Stamplecoskie, K. G.; Kamat, P. V. Size-Dependent Photovoltaic Performance of CuInS2 Quantum Dot-Sensitized Solar Cells. *Chem. Mater.* **2014**, *26* (24), 7221−7228.

(79) Andrei, V.; Ucoski, G. M.; Pornrungroj, C.; Uswachoke, C.; Wang, Q.; Achilleos, D. S.; Kasap, H.; Sokol, K. P.; Jagt, R. A.; Lu, H.; Lawson, T.; Wagner, A.; Pike, S. D.; Wright, D. S.; Hoye, R. L. Z.; MacManus-Driscoll, J. L.; Joyce, H. J.; Friend, R. H.; Reisner, E. Floating perovskite-BiVO4 devices for scalable solar fuel production. *Nature* **2022**, *608* (7923), 518−522.

(80) Teitsworth, T. S.; Hill, D. J.; Litvin, S. R.; Ritchie, E. T.; Park, J.-S.; Custer, J. P.; Taggart, A. D.; Bottum, S. R.; Morley, S. E.; Kim, S.; McBride, J. R.; Atkin, J. M.; Cahoon, J. F. Water splitting with silicon p-i-n superlattices suspended in solution. *Nature* **2023**, *614* (7947), 270−274.

(81) Moss, B.; Wang, Q.; Butler, K. T.; Grau-Crespo, R.; Selim, S.; Regoutz, A.; Hisatomi, T.; Godin, R.; Payne, D. J.; Kafizas, A.; Domen, K.; Steier, L.; Durrant, J. R. Linking in situ charge accumulation to electronic structure in doped SrTiO3 reveals design principles for hydrogen-evolving photocatalysts. *Nat. Mater.* **2021**, *20* (4), 511−517.

(82) Kim, T. W.; Choi, K. S. Nanoporous BiVO4 Photoanodes with Dual-Layer Oxygen Evolution Catalysts for Solar Water Splitting. *Science* **2014**, *343* (6174), 990−994.

(83) Pandey, A.; Guyot-Sionnest, P. Slow Electron Cooling in Colloidal Quantum Dots. *Science* **2008**, *322* (5903), 929−932.

(84) Wu, H.-L.; Li, X.-B.; Tung, C.-H.; Wu, L.-Z. Recent Advances in Sensitized Photocathodes: From Molecular Dyes to Semiconducting Quantum Dots. *Adv. Sci.* **2018**, *5* (4), 1700684.

(85) Zhang, J. H.; Zhang, M.; Dong, Y. Y.; Bai, C. C.; Feng, Y. Q.; Jiao, L.; Lv, H. J. CdTe/CdSe-sensitized photocathode coupling with Ni-substituted polyoxometalate catalyst for photoelectrochemical generation of hydrogen. *Nano Res.* **2022**, *15* (2), 1347−1354.

(86) Luo, B.; Liu, J.; Guo, H.; Liu, X.; Song, R.; Shen, K.; Wang, Z. M.; Jing, D.; Selopal, G. S.; Rosei, F. High efficiency photoelectrochemical hydrogen generation using eco-friendly Cu doped Zn-In-Se colloidal quantum dots. *Nano Energy* **2021**, *88*, 106220.

(87) Ghorpade, U. V.; Suryawanshi, M. P.; Shin, S. W.; Kim, J.; Kang, S. H.; Ha, J.-S.; Kolekar, S. S.; Kim, J. H. Unassisted visible solar water splitting with efficient photoelectrodes sensitized by quantum dots synthesized via an environmentally friendly eutectic solvent-mediated approach. *J. Mater. Chem. A* **2018**, *6* (45), 22566−22579.

(88) Gao, Y.; Wang, J.; Mo, S.; Wang, F.; Long, F.; Zou, Z. Synthesis of High-Quality Wurtzite Cu2ZnSn(S1-x,Sex)4 Nanocrystals With Non-Toxic Selenium Precursor and the Photoelectrochemical Performance of ZnO NAs/CZTSSe Heterojunction. *Solar RRL* **2018**, *2* (7), 1800015.

(89) Zhao, H. G.; Liu, G. J.; Vidal, F.; Wang, Y. Q.; Vomiero, A. Colloidal thick-shell pyramidal quantum dots for efficient hydrogen production. *Nano Energy* **2018**, *53*, 116−124.

(90) Li, S.; Jung, S. M.; Chung, W.; Seo, J. W.; Kim, H.; Park, S. I.; Lee, H. C.; Han, J. S.; Ha, S. B.; Kim, I. Y.; In, S. I.; Kim, J. Y.; Yang, J. Defect engineering of ternary Cu-In-Se quantum dots for boosting photo-electrochemical hydrogen generation. *Carbon Energy* **2023**, *5* (12), No. e384.

(91) Guo, H.; Liu, J.; Luo, B.; Huang, X.; Yang, J.; Chen, H.; Shi, L.; Liu, X.; Benetti, D.; Zhou, Y.; Selopal, G. S.; Rosei, F.; Wang, Z.; Niu, X. Unlocking the effects of Cu doping in heavy-metal-free AgIn5S8 quantum dots for highly efficient photoelectrochemical solar energy conversion. *J. Mater. Chem. C* **2021**, *9* (30), 9610−9618.

(92) Ng, C.; Yun, J.-H.; Tan, H. L.; Wu, H.; Amal, R.; Ng, Y. H. A dual-electrolyte system for photoelectrochemical hydrogen generation using CuInS2-In2O3-TiO2 nanotube array thin film. *Sci. China Mater.* **2018**, *61* (6), 895−904.

(93) Kim, J.; Jang, Y. J.; Baek, W.; Lee, A. R.; Kim, J. Y.; Hyeon, T.; Lee, J. S. Highly Efficient Photoelectrochemical Hydrogen Production Using Nontoxic CuIn1.5Se3 Quantum Dots with ZnS/SiO2 Double Overlayers. *ACS Appl. Mater. Interfaces* **2022**, *14* (1), 603−610.

(94) Kim, J. S.; Baek, S. K.; Kim, Y. B.; Do, H. W.; Kwon, Y. H.; Cho, S. W.; Yun, Y. D.; Yoon, J. H.; Lee, H.-B.-R.; Kim, S.-W.; Cho, H. K. Copper indium selenide water splitting photoanodes with artificially designed heterophasic blended structure and their high photo-electrochemical performances. *Nano Energy* **2018**, *46*, 1−10.

(95) Tong, X.; Zhou, Y.; Jin, L.; Basu, K.; Adhikari, R.; Selopal, G. S.; Tong, X.; Zhao, H.; Sun, S.; Vomiero, A.; Wang, Z. M.; Rosei, F. Heavy metal-free, near-infrared colloidal quantum dots for efficient photo-electrochemical hydrogen generation. *Nano Energy* **2017**, *31*, 441−449.

(96) Li, F.; Zhang, M.; Benetti, D.; Shi, L.; Besteiro, L. V.; Zhang, H.; Liu, J.; Selopal, G. S.; Sun, S.; Wang, Z.; Wei, Q.; Rosei, F. Green", gradient multi-shell CuInSe2/(CuInSexS1-x)5/CuInS2 quantum dots for photo-electrochemical hydrogen generation. *Appl. Catal., B* **2021**, *280*, 119402.

(97) Wang, R.; Tong, X.; Channa, A. I.; Zeng, Q.; Sun, J.; Liu, C.; Li, X.; Xu, J.; Lin, F.; Selopal, G. S.; Rosei, F.; Zhang, Y.; Wu, J.; Zhao, H.; Vomiero, A.; Sun, X.; Wang, Z. M. Environmentally friendly Mn-alloyed core/shell quantum dots for high-efficiency photoelectrochemical cells. *J. Mater. Chem. A* **2020**, *8* (21), 10736−10741.

(98) Zhao, H. G.; Zhang, H.; Liu, G. J.; Tong, X.; Liu, J. B.; Selopal, G. S.; Wang, Y. Q.; Wang, Z. M. M.; Sun, S. H.; Rosei, F. Ultra-small colloidal heavy-metal-free nanoplatelets for efficient hydrogen generation. *Appl. Catal., B* **2019**, *250*, 234−241.

(99) Sun, X.; Zhang, X.; Xie, Y. Surface Defects in Two-Dimensional Photocatalysts for Efficient Organic Synthesis. *Matter* **2020**, *2* (4), 842−861.

(100) Xiao, Y. Q.; Feng, C.; Fu, J.; Wang, F. Z.; Li, C. L.; Kunzelmann, V. F.; Jiang, C. M.; Nakabayashi, M.; Shibata, N.; Sharp, I. D.; Domen, K.; Li, Y. B. Band structure engineering and defect control of Ta3N5 for

efficient photoelectrochemical water oxidation. *Nat. Catal.* **2020**, *3* (11), 932−940.

(101) Gao, W.; Li, S.; He, H.; Li, X.; Cheng, Z.; Yang, Y.; Wang, J.; Shen, Q.; Wang, X.; Xiong, Y.; Zhou, Y.; Zou, Z. Vacancy-defect modulated pathway of photoreduction of CO2 on single atomically thin AgInP2S6 sheets into olefiant gas. *Nat. Commun.* **2021**, *12* (1), 4747.

(102) Kelkar, S.; Ballal, C.; Deshpande, A.; Warule, S.; Ogale, S. Quantum dot CdS coupled Cd2SnO4 photoanode with high photoelectrochemical water splitting efficiency. *J. Mater. Chem. A* **2013**, *1* (40), 12426−12431.

(103) Jiang, A. Q.; Guo, H.; Yu, S.; Zhang, F. Y.; Shuai, T. Y.; Ke, Y. B.; Yang, P.; Zhou, Y. Dual charge-accepting engineering modified AgIn5S8/CdS quantum dots for efficient photocatalytic hydrogen evolution overall H2S splitting. *Appl. Catal., B* **2023**, *332*, 122747.

(104) Fan, X. B.; Yu, S.; Zhan, F.; Li, Z. J.; Gao, Y. J.; Li, X. B.; Zhang, L. P.; Tao, Y.; Tung, C. H.; Wu, L. Z. Nonstoichiometric Cu(x) In(y) S Quantum Dots for Efficient Photocatalytic Hydrogen Evolution. *ChemSusChem* **2017**, *10* (24), 4833−4838.

(105) Liu, Z.; Liu, J.; Huang, Y.; Li, J.; Yuan, Y.; Ye, H.; Zhu, D.; Wang, Z.; Tang, A. From one-dimensional to two-dimensional wurtzite CuGaS2nanocrystals: non-injection synthesis and photocatalytic evolution. *Nanoscale* **2019**, *11* (1), 158−169.

(106) Colombara, D.; Elanzeery, H.; Nicoara, N.; Sharma, D.; Claro, M.; Schwarz, T.; Koprek, A.; Wolter, M. H.; Melchiorre, M.; Sood, M.; Valle, N.; Bondarchuk, O.; Babbe, F.; Spindler, C.; Cojocaru-Miredin, O.; Raabe, D.; Dale, P. J.; Sadewasser, S.; Siebentritt, S. Chemical instability at chalcogenide surfaces impacts chalcopyrite devices well beyond the surface. *Nat. Commun.* **2020**, *11* (1), 3634.

(107) Cahen, D.; Gilet, J.-M.; Schmitz, C.; Chernyak, L.; Gartsman, K.; Jakubowicz, A. Room-Temperature, Electric Field-Induced Creation of Stable Devices in CuInSe2 Crystals. *Science* **1992**, *258* (5080), 271−274.

(108) Qu, S.; Yuan, X.; Li, Y.; Li, X.; Zhou, X.; Xue, X.; Zhang, K.; Xu, J.; Yuan, C. Aqueous synthesis of composition-tuned defects in CuInSe2 nanocrystals for enhanced visible-light photocatalytic H2 evolution. *Nanoscale Adv.* **2021**, *3* (8), 2334−2342.

(109) Franklin, A. D. DEVICE TECHNOLOGY. Nanomaterials in transistors: From high-performance to thin-film applications. *Science* **2015**, *349* (6249), aab2750.

(110) Ko, H.; Takei, K.; Kapadia, R.; Chuang, S.; Fang, H.; Leu, P. W.; Ganapathi, K.; Plis, E.; Kim, H. S.; Chen, S. Y.; Madsen, M.; Ford, A. C.; Chueh, Y. L.; Krishna, S.; Salahuddin, S.; Javey, A. Ultrathin compound semiconductor on insulator layers for high-performance nanoscale transistors. *Nature* **2010**, *468* (7321), 286−9.

(111) Shimoda, T.; Matsuki, Y.; Furusawa, M.; Aoki, T.; Yudasaka, I.; Tanaka, H.; Iwasawa, H.; Wang, D.; Miyasaka, M.; Takeuchi, Y. Solution-processed silicon films and transistors. *Nature* **2006**, *440* (7085), 783−786.

(112) Jacobson, M. Z. Review of solutions to global warming, air pollution, and energy security. *Energy Environ. Sci.* **2009**, *2* (2), 148−173.

(113) Vicarelli, L.; Vitiello, M. S.; Coquillat, D.; Lombardo, A.; Ferrari, A. C.; Knap, W.; Polini, M.; Pellegrini, V.; Tredicucci, A. Graphene field-effect transistors as room-temperature terahertz detectors. *Nat. Mater.* **2012**, *11* (10), 865−871.

(114) Ferain, I.; Colinge, C. A.; Colinge, J. P. Multigate transistors as the future of classical metal-oxide-semiconductor field-effect transistors. *Nature* **2011**, *479* (7373), 310−6.

(115) Desai, S. B.; Madhvapathy, S. R.; Sachid, A. B.; Llinas, J. P.; Wang, Q.; Ahn, G. H.; Pitner, G.; Kim, M. J.; Bokor, J.; Hu, C.; Wong, H.-S. P.; Javey, A. MoS2 transistors with 1-nanometer gate lengths. *Science* **2016**, *354* (6308), 99−102.

(116) Jia, X.; Fuentes-Hernandez, C.; Wang, C.-Y.; Park, Y.; Kippelen, B. Stable organic thin-film transistors. *Sci. Adv.* **2018**, *4* (1), No. eaao1705.

(117) Ning, Z.; Voznyy, O.; Pan, J.; Hoogland, S.; Adinolfi, V.; Xu, J.; Li, M.; Kirmani, A. R.; Sun, J. P.; Minor, J.; Kemp, K. W.; Dong, H.; Rollny, L.; Labelle, A.; Carey, G.; Sutherland, B.; Hill, I.; Amassian, A.;

Liu, H.; Tang, J.; Bakr, O. M.; Sargent, E. H. Air-stable n-type colloidal quantum dot solids. *Nat. Mater.* **2014**, *13* (8), 822−8.

(118) Moon, H.; Lee, C.; Lee, W.; Kim, J.; Chae, H. Stability of Quantum Dots, Quantum Dot Films, and Quantum Dot Light-Emitting Diodes for Display Applications. *Adv. Mater.* **2019**, *31* (34), 1804294.

(119) Talapin, D. V.; Lee, J. S.; Kovalenko, M. V.; Shevchenko, E. V. Prospects of Colloidal Nanocrystals for Electronic and Optoelectronic Applications. *Chem. Rev.* **2010**, *110* (1), 389−458.

(120) Choi, J.-H.; Wang, H.; Oh, S. J.; Paik, T.; Sung, P.; Sung, J.; Ye, X.; Zhao, T.; Diroll, B. T.; Murray, C. B.; Kagan, C. R. Exploiting the colloidal nanocrystal library to construct electronic devices. *Science* **2016**, *352* (6282), 205−208.

(121) Dolzhnikov, D. S.; Zhang, H.; Jang, J.; Son, J. S.; Panthani, M. G.; Shibata, T.; Chattopadhyay, S.; Talapin, D. V. Composition-matched molecular "solders" for semiconductors. *Science* **2015**, *347* (6220), 425−428.

(122) Wang, Y.; Fedin, I.; Zhang, H.; Talapin, D. V. Direct optical lithography of functional inorganic nanomaterials. *Science* **2017**, *357* (6349), 385−388.

(123) Talapin, D. V.; Murray, C. B. PbSe nanocrystal solids for n- and p-channel thin film field-effect transistors. *Science* **2005**, *310* (5745), 86−9.

(124) Lee, H. J.; Im, S.; Jung, D.; Kim, K.; Chae, J. A.; Lim, J.; Park, J. W.; Shin, D.; Char, K.; Jeong, B. G.; Park, J.-S.; Hwang, E.; Lee, D. C.; Park, Y.-S.; Song, H.-J.; Chang, J. H.; Bae, W. K. Coherent heteroepitaxial growth of I-III-VI2 Ag(In,Ga)S2 colloidal nanocrystals with near-unity quantum yield for use in luminescent solar concentrators. *Nat. Commun.* **2023**, *14* (1), 3779.

(125) Draguta, S.; McDaniel, H.; Klimov, V. I. Tuning carrier mobilities and polarity of charge transport in films of CuInSe(x)S(2-x) quantum dots. *Adv. Mater.* **2015**, *27* (10), 1701−5.

(126) Yarema, O.; Yarema, M.; Bozyigit, D.; Lin, W. M.; Wood, V. Independent Composition and Size Control for Highly Luminescent Indium-Rich Silver Indium Selenide Nanocrystals. *ACS Nano* **2015**, *9* (11), 11134−42.

(127) Zhong, H.; Wang, Z.; Bovero, E.; Lu, Z.; van Veggel, F. C. J. M.; Scholes, G. D. Colloidal CuInSe2 Nanocrystals in the Quantum Confinement Regime: Synthesis, Optical Properties, and Electro-luminescence. *J. Phys. Chem. C* **2011**, *115* (25), 12396−12402.

(128) Wang, H.; Butler, D. J.; Straus, D. B.; Oh, N.; Wu, F.; Guo, J.; Xue, K.; Lee, J. D.; Murray, C. B.; Kagan, C. R. Air-Stable CuInSe2 Nanocrystal Transistors and Circuits via Post-Deposition Cation Exchange. *ACS Nano* **2019**, *13* (2), 2324−2333.

(129) Yun, H. J.; Lim, J.; Fuhr, A. S.; Makarov, N. S.; Keene, S.; Law, M.; Pietryga, J. M.; Klimov, V. I. Charge-Transport Mechanisms in CuInSexS2-x Quantum-Dot Films. *ACS Nano* **2018**, *12* (12), 12587−12596.

(130) Zito, J.; Infante, I. The Future of Ligand Engineering in Colloidal Semiconductor Nanocrystals. *Acc. Chem. Res.* **2021**, *54* (7), 1555−1564.

(131) Wang, W.; Zhang, M.; Pan, Z.; Biesold, G. M.; Liang, S.; Rao, H.; Lin, Z.; Zhong, X. Colloidal Inorganic Ligand-Capped Nanocrystals: Fundamentals, Status, and Insights into Advanced Functional Nanodevices. *Chem. Rev.* **2022**, *122* (3), 4091−4162.

(132) Ong, W.-L.; Rupich, S. M.; Talapin, D. V.; McGaughey, A. J.; Malen, J. A. Surface chemistry mediates thermal transport in three-dimensional nanocrystal arrays. *Nat. Mater.* **2013**, *12* (5), 410−415.

(133) Kim, T.; Kim, K.-H.; Kim, S.; Choi, S.-M.; Jang, H.; Seo, H.-K.; Lee, H.; Chung, D.-Y.; Jang, E. Efficient and stable blue quantum dot light-emitting diode. *Nature* **2020**, *586* (7829), 385−389.

(134) Jung, H.; Ahn, N.; Klimov, V. I. Prospects and challenges of colloidal quantum dot laser diodes. *Nat. Photonics* **2021**, *15* (9), 643−655.

(135) Xu, H.; Song, J.; Zhou, P.; Song, Y.; Xu, J.; Shen, H.; Fang, S.; Gao, Y.; Zuo, Z.; Pina, J. M.; Voznyy, O.; Yang, C.; Hu, Y.; Li, J.; Du, J.; Sargent, E. H.; Fan, F. Dipole-dipole-interaction-assisted self-assembly of quantum dots for highly efficient light-emitting diodes. *Nat. Photonics* **2024**, *18* (2), 186−191.

(136) Dai, X. L.; Zhang, Z. X.; Jin, Y. Z.; Niu, Y.; Cao, H. J.; Liang, X. Y.; Chen, L. W.; Wang, J. P.; Peng, X. G. Solution-processed, high-performance light-emitting diodes based on quantum dots. *Nature* **2014**, *515* (7525), 96−99.

(137) Hanifi, D. A.; Bronstein, N. D.; Koscher, B. A.; Nett, Z.; Swabeck, J. K.; Takano, K.; Schwartzberg, A. M.; Maserati, L.; Vandewal, K.; van de Burgt, Y.; Salleo, A.; Alivisatos, A. P. Redefining near-unity luminescence in quantum dots with photothermal threshold quantum yield. *Science* **2019**, *363* (6432), 1199−1202.

(138) Gao, Y.; Li, B.; Liu, X. A.; Shen, H. B.; Song, Y.; Song, J. J.; Yan, Z. J.; Yan, X. H.; Chong, Y. H.; Yao, R. Y.; Wang, S. J.; Li, L. S.; Fan, F. J.; Du, Z. L. Minimizing heat generation in quantum dot light-emitting diodes by increasing quasi-Fermi-level splitting. *Nat. Nanotechnol.* **2023**, *18* (10), 1168−1174.

(139) Xia, C. H.; Tamarat, P.; Hou, L.; Busatto, S.; Meeldijk, J. D.; Donega, C. D.; Lounis, B. Unraveling the Emission Pathways in Copper Indium Sulfide Quantum Dots. *ACS Nano* **2021**, *15* (11), 17573−17581.

(140) Zhong, H.; Bai, Z.; Zou, B. Tuning the Luminescence Properties of Colloidal I-III-VI Semiconductor Nanocrystals for Optoelectronics and Biotechnology Applications. *J. Phys. Chem. Lett.* **2012**, *3* (21), 3167−3175.

(141) Chen, B.; Pradhan, N.; Zhong, H. From Large-Scale Synthesis to Lighting Device Applications of Ternary I-III-VI Semiconductor Nanocrystals: Inspiring Greener Material Emitters. *J. Phys. Chem. Lett.* **2018**, *9* (2), 435−445.

(142) Tong, X.; Kong, X.-T.; Zhou, Y.; Navarro-Pardo, F.; Selopal, G. S.; Sun, S.; Govorov, A. O.; Zhao, H.; Wang, Z. M.; Rosei, F. Near-Infrared, Heavy Metal-Free Colloidal "Giant" Core/Shell Quantum Dots. *Adv. Energy Mater.* **2018**, *8* (2), 1701432.

(143) Allen, P. M.; Bawendi, M. G. Ternary I- III- VI quantum dots luminescent in the red to near-infrared. *J. Am. Chem. Soc.* **2008**, *130* (29), 9240−9241.

(144) Nose, K.; Omata, T.; Otsuka-Yao-Matsuo, S. Colloidal Synthesis of Ternary Copper Indium Diselenide Quantum Dots and Their Optical Properties. *J. Phys. Chem. C* **2009**, *113* (9), 3455−3460.

(145) Cassette, E.; Pons, T.; Bouet, C.; Helle, M.; Bezdetnaya, L.; Marchal, F.; Dubertret, B. Synthesis and characterization of near-infrared Cu- In- Se/ZnS core/shell quantum dots for in vivo imaging. *Chem. Mater.* **2010**, *22* (22), 6117−6124.

(146) Park, J.; Dvoracek, C.; Lee, K. H.; Galloway, J. F.; Bhang, H. E.; Pomper, M. G.; Searson, P. C. CuInSe/ZnS core/shell NIR quantum dots for biomedical imaging. *Small* **2011**, *7* (22), 3148−52.

(147) Wang, L.; Cao, X.; Liu, Z.; Wang, Y.; Xiong, P.; Li, X.; Gao, W.; Tang, B. Dual near infrared emission in Ag2Se quantum dots via Pb doping for broadband mini light-emitting diodes. *Chem. Commun.* **2022**, *58* (60), 8432−8435.

(148) Wang, L.; Cao, X.; Liu, Z.; Wang, Y.; Xiong, P.; Gao, W.; Tang, B. Enhancement and broadening of near infrared photoluminescence in Ag2X (X= S, Se) quantum dots via Cd doping for mini light-emitting diodes towads non-invasive bioimaging. *J. Lumin.* **2022**, *252*, 119325.

(149) Huang, W.-T.; Yoon, S.-Y.; Wu, B.-H.; Lu, K.-M.; Lin, C.-M.; Yang, H.; Liu, R.-S. Ultra-broadband near-infrared emission CuInS2/ ZnS quantum dots with high power efficiency and stability for the theranostic applications of mini light-emitting diodes. *Chem. Commun.* **2020**, *56* (59), 8285−8288.

(150) Kim, M.; Lee, G. J.; Choi, C.; Kim, M. S.; Lee, M.; Liu, S.; Cho, K. W.; Kim, H. M.; Cho, H.; Choi, M. K.; Lu, N.; Song, Y. M.; Kim, D.-H. An aquatic-vision-inspired camera based on a monocentric lens and a silicon nanorod photodiode array. *Nat. Electronics* **2020**, *3* (9), 546−553.

(151) Geiger, S.; Michon, J.; Liu, S.; Qin, J.; Ni, J.; Hu, J.; Gu, T.; Lu, N. Flexible and Stretchable Photonics: The Next Stretch of Opportunities. *ACS Photonics* **2020**, *7* (10), 2618−2635.

(152) Cai, S.; Xu, X.; Yang, W.; Chen, J.; Fang, X. Materials and Designs for Wearable Photodetectors. *Adv. Mater.* **2019**, *31* (18), 1808138.

(153) Michel, J.; Liu, J.; Kimerling, L. C. High-performance Ge-on-Si photodetectors. *Nat. Photonics* **2010**, *4* (8), 527−534.

(154) Sukhovatkin, V.; Hinds, S.; Brzozowski, L.; Sargent, E. H. Colloidal quantum-dot photodetectors exploiting multiexciton generation. *Science* **2009**, *324* (5934), 1542−4.

(155) Roy, K.; Padmanabhan, M.; Goswami, S.; Sai, T. P.; Ramalingam, G.; Raghavan, S.; Ghosh, A. Graphene-MoS2 hybrid structures for multifunctional photoresponsive memory devices. *Nat. Nanotechnol.* **2013**, *8* (11), 826−830.

(156) Mueller, T.; Xia, F.; Avouris, P. Graphene photodetectors for high-speed optical communications. *Nat. Photonics* **2010**, *4* (5), 297−301.

(157) Guo, R. Q.; Huang, F.; Zheng, K. B.; Pullerits, T.; Tian, J. J. CuInSe2 Quantum Dots Hybrid Hole Transfer Layer for Halide Perovskite Photodetectors. *ACS Appl. Mater. Interfaces* **2018**, *10* (41), 35656−35663.

(158) Liu, M.; Yazdani, N.; Yarema, M.; Jansen, M.; Wood, V.; Sargent, E. H. Colloidal quantum dot electronics. *Nat. Electronics* **2021**, *4* (8), 548−558.

(159) Park, Y. S.; Roh, J.; Diroll, B. T.; Schaller, R. D.; Klimov, V. I. Colloidal quantum dot lasers. *Nat. Rev. Mater.* **2021**, *6* (5), 382−401.

(160) Kim, J. Y.; Voznyy, O.; Zhitomirsky, D.; Sargent, E. H. 25th Anniversary Article: Colloidal Quantum Dot Materials and Devices: A Quarter-Century of Advances. *Adv. Mater.* **2013**, *25* (36), 4986−5010.

(161) McDonald, S. A.; Konstantatos, G.; Zhang, S.; Cyr, P. W.; Klem, E. J.; Levina, L.; Sargent, E. H. Solution-processed PbS quantum dot infrared photodetectors and photovoltaics. *Nat. Mater.* **2005**, *4* (2), 138−42.

(162) Clifford, J. P.; Konstantatos, G.; Johnston, K. W.; Hoogland, S.; Levina, L.; Sargent, E. H. Fast, sensitive and spectrally tuneable colloidal-quantum-dot photodetectors. *Nat. Nanotechnol.* **2009**, *4* (1), 40−4.

(163) Liu, H.; Yu, M. M.; Qn, F. L.; Feng, W.; Hu, P. A. Two-Dimensional Nonlayered CuInSe2 Nanosheets for High-Performance Photodetectors. *ACS Appl. Nano Mater.* **2018**, *1* (10), 5414−5418.

(164) Bi, W.; Zhou, M.; Ma, Z.; Zhang, H.; Yu, J.; Xie, Y. CuInSe2 ultrathin nanoplatelets: novel self-sacrificial template-directed synthesis and application for flexible photodetectors. *Chem. Commun.* **2012**, *48* (73), 9162−4.

(165) Lei, S.; Sobhani, A.; Wen, F.; George, A.; Wang, Q.; Huang, Y.; Dong, P.; Li, B.; Najmaei, S.; Bellah, J.; Gupta, G.; Mohite, A. D.; Ge, L.; Lou, J.; Halas, N. J.; Vajtai, R.; Ajayan, P. Ternary CuIn7Se11: towards ultra-thin layered photodetectors and photovoltaic devices. *Adv. Mater.* **2014**, *26* (45), 7666−72.